The Astronomical Journal, 136:1147–1170, 2008 September doi:10.1088/0004-6256/136/3/1147
© 2008. The American Astronomical Society. All rights reserved. Printed in the U.S.A.

THE NUCLEUS OF THE SAGITTARIUS DSPH GALAXY AND M54: A WINDOW ON THE PROCESS OF GALAXY NUCLEATION

M. Bellazzini[1], R. A. Ibata[2], S. C. Chapman[3,10], A. D. Mackey[4], L. Monaco[5], M. J. Irwin[6], N. F. Martin[7], G. F. Lewis[8], and E. Dalessandro[9,11]

[1] INAF—Osservatorio Astronomico di Bologna, via Ranzani 1, 40127, Bologna, Italy; michele.bellazzini@oabo.inaf.it
[2] Observatoire Astronomique, Université de Strasbourg, CNRS, 11, rue de l'Université, F-67000 Strasbourg, France; ibata@astro.u-strasbg.fr
[3] Institute of Astronomy, Madingley Road, Cambridge CB3 0HA, UK; schapman@ast.cam.ac.uk
[4] Institute for Astronomy, University of Edinburgh, Royal Observatory, Blackford Hill, Edinburgh EH9 3HJ, UK; dmy@roe.ac.uk
[5] European Southern Observatory, Alonso de Cordova 3107, Casilla 19001, Santiago, Chile; lmonaco@eso.org
[6] Institute of Astronomy, Madingley Road, Cambridge CB3 0HA, UK; mike@ast.cam.ac.uk
[7] Max-Planck-Institut für Astronomie, Königstuhl 17, D-69117 Heidelberg, Germany; martin@mpia-hd.mpg.de
[8] Institute of Astronomy, School of Physics, A29 University of Sydney, NSW 2006, Australia; gfl@physics.usyd.edu.au
[9] Dipartimento di Astronomia, Università di Bologna, via Ranzani 1, 40127, Bologna, Italy; emanuele.dalessandr2@unibo.it
[10] University of Victoria, Victoria, BC, V8W 3P6, Canada
[11] ASI, Centro di Geodesia Spaziale, contrada Terlecchia, I-75100, Matera, Italy
Received 2008 January 28; accepted 2008 June 30; published 2008 August 11

ABSTRACT

We present the results of a thorough study of the nucleus of the Sgr dwarf spheroidal galaxy (Sgr dSph) and of the bright globular cluster M54 (NGC 6715) that resides within the same nucleus (Sgr,N). We have obtained accurate radial velocities and metallicity estimates for 1152 candidate red giant branch stars of Sgr and M54 lying within $\sim 9'$ from the center of the galaxy, from Keck/DEIMOS and VLT/FLAMES spectra of the infrared Ca II triplet. Using both velocity and metallicity information we selected two samples of 425 and 321 very likely members of M54 and of Sgr,N, respectively. The two considered systems display significantly different velocity dispersion profiles. M54 has a steeply decreasing profile from $r = 0'$, where $\sigma \simeq 14.2$ km s^{-1}, to $r \simeq 3'.5$ where it reaches $\sigma \simeq 5.3$ km s^{-1}, then it appears to rise again to $\sigma \simeq 10$ km s^{-1} at $r \sim 7'$. In contrast Sgr,N has a uniformly flat profile at $\sigma \simeq 9.6$ km s^{-1} over the whole $0' \leqslant r \leqslant 9'$ range. Using data from the literature we show that the velocity dispersion of Sgr remains constant at least out to $r \sim 100'$ and there is no sign of the transition between the outer flat-luminosity-profile core and the inner nucleus in the velocity profile. These results, together with a re-analysis of the surface brightness profile of Sgr,N and a suite of dedicated N-body simulations, provide very strong support for the hypothesis that the nucleus of Sgr formed independently of M54, which probably plunged to its present position, coincident with Sgr,N, because of significant decay of the original orbit due to dynamical friction.

Key words: galaxies: dwarf – galaxies: individual (Sgr dSph) – galaxies: nuclei – globular clusters: individual (NGC 6715) – stars: kinematics

Online-only material: color figures

1. INTRODUCTION

The occurrence of stellar nuclei at the photometric center of several dwarf elliptical galaxies has been the subject of statistical investigations since the pioneering study by Binggeli et al. (1985) and Binggeli et al. (1987), and nucleated dwarf ellipticals (dE,N) have become a generally recognized and well-studied class of galaxies in their own right (see Gallagher & Wyse 1994; Ferguson & Binggeli 1994, and references therein). In the last few years the results from systematic studies performed with the instrumentation on board the *Hubble Space Telescope* (*HST*) have revolutionized the field, providing strong evidence supporting the possibility of an intimate connection between the process of nucleation and the process of galaxy formation as a whole. In particular:

1. It was generally accepted that stellar nuclei occurred in a significant but minor fraction of dwarf elliptical galaxies ($\sim$25% Binggeli et al. 1985); on the other hand, the high-resolution *HST* analysis of a large and well selected sample of Virgo dEs by Côté et al. (2006, hereafter C06) has revealed that the fraction of dE,Ns (f_n) can be as high as $66\% \leqslant f_n \leqslant 87\%$. Strong support to a significant upward revision of f_n comes also from the recent ground-based study by Grant et al. (2005). Hence, nucleation appears as the natural status of dEs instead of an exceptional occurrence (see C06 for details and discussion).
2. An *HST* study of a large sample of Sa-Sd galaxies by Böker et al. (2004) found that a similarly high fraction of stellar nuclei is found also among these late-type spirals, $f_n \simeq 77\%$. In general, the most recent studies agree in finding a fraction of nucleation larger than 50% in any kind of galaxy (see, for example, Carollo et al. 1998; Balcells et al. 2007; Ferrarese & Côté 2006; Böker 2008, and references therein), with the only exception of those brighter than $M_B \simeq -20.3$ mag (Ferrarese & Côté 2006, hereafter FC06). Hence, nucleation seems to occur very frequently in both dwarf and giant galaxies (see Graham & Guzmán 2003, and references therein, for a deeper discussion of the dwarf/giant dichotomy).
3. Stellar galactic nuclei are found to obey the same scaling relation that links supermassive black holes (SBHs) with their host galaxies (Wehner & Harris 2006, C06, FC06). It has been suggested that "...SBHs and stellar nuclei are nothing but complementary incarnations of Central Massive Objects—they likely share a common formation mechanism and follow a similar evolutionary path..."

(FC06). In this view, the accumulation of a compact overdensity of baryons at the very center would be a common process during galaxy formation, while its further evolution into a SBH or a stellar nucleus would depend on various "local" circumstances.

4. The similarity between stellar nuclei, the brightest globular clusters, and the recently discovered ultracompact dwarf (UCD) galaxies (Drinkwater et al. 2003) clearly suggests possible links among these classes of stellar systems (Freeman 1993; Lotz et al. 2001, 2004; Bassino et al. 1994; Hasegan et al. 2005; Federici et al. 2007; Böker 2008). In particular it has been suggested either that nuclei can form by the merging of pre-existing globular clusters (Lotz et al. 2001, and references therein), or that some objects currently classified as globular clusters may be, in fact, galactic nuclei—the only relics of the tidal shredding of their host galaxies that once orbited the Milky Way and/or M31 (see Mackey & van den Bergh 2005; Federici et al. 2007; Brodie & Strader 2006 (hereafter BS), and references therein), or even that most/all globulars were nuclei of Galactic building blocks (i.e., dwarf galaxies, see Freeman 1993; Freeman & Bland-Hawthorn 2002; Böker 2008, BS, and references therein).

Within the scenario briefly outlined above, the crucial relevance of any independent observational fact that may provide some insight on the process of nucleation is clearly manifest. The mechanisms for the formation of stellar nuclei that have been suggested until now belong to two broad classes: (a) the orbital decay and merging at the center of the parent galaxies of pre-existing stellar systems (star clusters), and (b) the accumulation of gas (of various origins) in the very center of a galaxy and its subsequent transformation into stars (see Grant et al. 2005 for a detailed description of various proposed flavors of these classes of models).

At present, all the observational constraints we have in hand come from the study of the integrated properties of samples of distant galaxies/nuclei. The nearest galaxies that are known to host a stellar nucleus are M32, M33, and NGC 205, in the Local Group. Even in the most favorable case of NGC 205, the structure of the nucleus can be studied in some detail, but it can be resolved into individual stars only partially, even with *HST* imaging (Valluri et al. 2005). In this context the case of the Sagittarius dwarf spheroidal galaxy (Sgr dSph, Ibata et al. 1994) constitutes an absolute *unicum* (Monaco et al. 2005a, hereafter M05a).

The Sgr dSph is a dwarf satellite ($L \sim 2-5\times10^7\,L_\odot$) of the Milky Way (Ibata et al. 1997) whose main body is at $D_\odot = 26.3 \pm 1.8$ kpc from Earth and $R_{GC} \simeq 18.7$ kpc from the center of the Galaxy (Monaco et al. 2004). It is devoid of gas (Burton & Lockman 1999). Its stellar content is dominated by an intermediate-age (∼6–8 Gyr old, see Bellazzini et al. 2006a, and references therein), metal-rich ($\langle Z\rangle \sim \frac{2}{5}\,Z_\odot$, Monaco et al. 2005b, hereafter M05b, and references therein) population. A small fraction (∼=10%) of old and metal-poor stars is also present (Monaco et al. 2003). The Sgr dSph is currently being destroyed by the galactic tidal field (Ibata et al. 1997). The tidally stripped stars form a huge and coherent tidal tail system that can be observed over the whole celestial sphere (Sgr Stream, see Ibata et al. 2001; Majewski et al. 2003, and references therein). There are four globular clusters within the main body of the Sgr galaxy (Ibata et al. 1994; Da Costa & Armandroff 1995; Montegriffo et al. 1998) and probably several others that have been stripped from the main body and are now associated with the Sgr Stream (Bellazzini et al. 2003a, 2003b; Carraro et al. 2007).

Particularly noticeable, however, is the very bright ($M_V = -10.0$, Harris 1996) metal-poor ([Fe/H] $= -1.55$) (Brown et al. 1999) globular cluster M54 (NGC 6715), located exactly at the center of the light distribution of the Sgr galaxy. For this reason, immediately after the discovery of the galaxy, it was suggested that M54 could be the actual nucleus of Sgr dSph (Bassino & Muzzio 1995; Sarajedini & Layden 1995). Some doubt on this hypothesis was advanced by Da Costa & Armandroff (1995) based on the fact that the integrated color of M54 is much bluer than that of its host galaxy, while the opposite was generally believed to occur in dE,Ns; however, Sarajedini & Layden (1997) noticed that there were exceptions to this rule. In fact, the latest studies suggest that the opposite may be true (Lotz et al. 2004, see also C06). Since the mean metallicity of M54 and of the population dominating the Sgr galaxy differ by one full dex, their red giant branch (RGB) stars (and in some cases also their horizontal branch stars, HB) can be easily discriminated from each other in a color—magnitude diagram (CMD); at the same magnitude the RGB of Sgr is much redder than that of M54. Selecting genuine Sgr stars in this way, Layden & Sarajedini (2000) and Majewski et al. (2003) independently found an overdensity of Sgr stars that appear concentric with M54 and have a similar spatial scale. Using the same technique and a very large optical photometry database, M05a demonstrated that Sgr actually has a nucleus of metal-rich stars (in the following we will refer to this structure as the *nucleus* of the Sagittarius galaxy, *Sgr,N* for brevity, if not otherwise stated). This stellar structure has the same center as M54, within the uncertainties, but it displays a different surface brightness (SB) profile, suggesting a different origin from the cluster. The strong incompleteness in the innermost ∼10″ prevented M05a from obtaining accurate estimates of the structural parameters of the Sgr nucleus: they derived $-10.0 \leqslant M_V \leqslant -7.6$, $\mu_V(0) \lesssim 18.5$ mag arcsec^{-2}, and, with a tentative fit of a King (1966) model, $r_c \lesssim 0.21'$ and $r_t \sim 17'$ (where $C = \log(r_t/r_c) \sim 1.9$; we will refine these parameters in Section 2). They also found that the observed properties of the nucleus of the Sgr galaxy were fully compatible with those of known nuclei of dwarf ellipticals. Moreover, the recent study by Siegel et al. (2007) has shown that, while the stellar budget of Sgr,N is dominated by the same intermediate-age population found in the surrounding galaxy, there is clear evidence of more recent and repeated episodes of star formation (not observed in extra-nuclear fields, Bellazzini et al. 2006a), pointing to a history of subsequent phases of re-accumulation of gas followed by star-formation bursts, which is very similar to what is observed by Rossa et al. (2006) in a large sample of distant galactic nuclei.

In any case, the key result of M05a is that Sgr is a nucleated galaxy independently of the presence of M54; even if one were able to remove the cluster from the galaxy by magic, a nucleus made of typical Sgr stars would still be there. To explain the strict spatial coincidence of M54 and the nucleus, M05a proposed two possibilities: (a) the nucleus formed *in situ* from processed Sgr gas that has fallen to the bottom of the galactic potential well, and M54 was (independently) driven into the same place by dynamical friction; (b) M54 was born in the present place (or was driven there as in case (a)) and formed a co-spatial overdensity of Sgr stars by capturing them (or the gas from which they formed) from the surroundings. The key difference between the two hypotheses can be summarized by the questions: Did M54

provide the mass seed around which the metal-rich nucleus of Sgr was assembled? Is M54 the main contributor of the mass budget in the innermost ∼100 pc of the Sgr galaxy?

Hypothesis (a) was found to be fully compatible with all the available information, while it was not possible to consider case (b) in more depth. In a recent paper, Mieske & Baumgardt (2007) studied in detail the process of the capture of "field" stars from an intervening star cluster and they concluded that, even in the most favorable cases, the fraction of stars captured in a Hubble time is negligible—less that 10^{-4} of the cluster mass. The range of conditions studied by Mieske & Baumgardt includes the "M54 within Sgr" case, hence their conclusions are fully applicable here. Nevertheless, the results of Mieske & Baumgardt do not exclude the possibility that M54 operates as a collector of processed gas at the center of Sgr.

However, it seems quite reasonable to expect that if case (b) is true, the stars of the Sgr,N structure should share the same kinematics as M54 stars, or, at least, their kinematics should be compatible with a mass-follows-light model, or, finally, their kinematics should be different from that of extra-nuclear Sgr stars, as they would be bound to M54 and would orbit within its potential (Gilmore et al. 2007). Note that M54 and Sgr,N are enclosed within the innermost 10′ of a galaxy whose core radius and limiting radius are as large as $r_c = 224' \pm 10'$ and $r_t = 1801' \pm 112'$, respectively (Majewski et al. 2003). Hence, even if the main body of Sgr is clearly undergoing tidal disruption the kinematics of the nuclear region should be unaffected and is consequently expected to provide a trustworthy insight on the inner mass distribution (Muñoz et al. 2008).

To follow up these ideas and to obtain a deeper insight into this unique case of a galactic nucleus that can be studied *in vivo* on a star-by-star basis, we performed an extensive spectroscopic survey principally aimed at the study of the kinematics of Sgr,N and M54. Here we present the main results of this survey. The plan of the paper is as follows. As a preliminary step we re-analyze the SB profile of Sgr,N with new data in Section 2. In Section 3 we describe the observation and data reduction of our spectroscopic survey, we test the reliability and the accuracy of our measures, the observed metallicity distribution is briefly discussed and, finally, the selection of the samples is described in detail. Section 4 is devoted to the kinematical analysis of the M54 and Sgr,N samples and in Section 5 we briefly present the results of a suite of N-body simulations aimed at the study of the orbital decay of M54 within the Sgr galaxy. Finally, in Section 6 we summarize and discuss our results.

2. REFINING THE STRUCTURAL PARAMETERS OF Sgr,N

To gain a better insight into the SB profile of Sgr,N, we reduced archive data obtained with the Wide Field Channel (WFC) of the Advanced Camera for Survey (ACS) on board of the *HST*. This is a set of short and long exposure F814W and F606W images of the center of M54, taken within the GO 10775 Treasury Program (Sarajedini et al. 2007). The relative and absolute photometry of individual stars has been obtained following the same steps as described in Sollima et al. (2007) for data taken from the same survey. Further details and the overall analysis of these data will be presented elsewhere; an independent study of the stellar populations of M54 and Sgr,N from the same images has been recently presented by Siegel et al. (2007). In the present context, we limit ourselves to complementing the SB profile of Sgr,N obtained by M05a with a couple of points in the innermost 10″, using the same methodology as M05a, and, as a consequence, to obtaining stronger constraints on the structural parameters of Sgr,N.

Table 1
SB Profile of the Innermost 60″ of Sgr

r_i (″)	r_f (″)	r_m (″)	μ_V (mag arcsec^{-2})	e_{μ_V} (mag arcsec^{-2})
0	5	3.01	16.1	0.3
0	10	5.35	16.6	0.2
10	20	14.30	18.3	0.3
20	40	27.84	20.0	0.4
40	60	49.78	21.7	0.6

Note. r_i and r_f are the limits of the bins, r_m is the average radius of the sample.

Figure 1 clearly shows that the new ACS photometry allows one to discriminate the RGBs of M54 and Sgr,N by color even in the innermost 10″. Using the selection illustrated in Figure 1 we were able to reliably measure the ratio of the density of tracer stars (RGB and asymptotic giant branch (AGB), in the present case) in the two samples in any given radial annulus $\rho_{\rm Sgr,N}/\rho_{\rm M54}$, as it scales as the ratio of the number of stars per annulus $N_{\rm Sgr,N}/N_{\rm M54}$. To avoid the inter-chip gap we used semi-annuli for $R > 10''$. The quantity $2.5\log(N_{\rm Sgr,N}/N_{\rm M54})$, in turn, scales as the difference in SB between the two systems (see M05a for details, and Renzini & Buzzoni 1986; Renzini & Fusi Pecci 1988, for the basis of the underlying evolutionary flux theorem).[12] No attempt was made to estimate the ellipticity of the system; as the system appears quite spherical at large radii (see M05a) we assumed spherical symmetry. The coordinates of the centers of M54 and Sgr,N, as derived from the 2σ clipped average X and Y of stars selected by color as in Figure 1, are found to coincide to within $<2''$, in excellent agreement with M05a. The effects of the radial variation of completeness on the density ratio should be practically null, as we selected the M54 and Sgr,N samples in the same (bright) magnitude range ($13.8 \leqslant$ F814W $\leqslant 16.4$). To convert the estimated SB differences into an absolute scale we adopted the best-fit model profile of M54 by Trager et al. (1995) as a "zero-point," consistent with M05a. In practice, for each observed $\Delta\mu^{\rm Sgr-M54}(R_i)$ we obtained the SB of Sgr,N at radius R_i, $\mu_V^{\rm Sgr}(R_i)$, as $\mu_V^{\rm Sgr}(R_i) = \mu_V^{\rm M54}(R_i) + \Delta\mu^{\rm Sgr-M54}(R_i)$. The derived portion of the profile is reported in Table 1 and plotted in Figure 2, together with the portions of the M54 and Sgr,N profiles derived by M05a.

The SB of Sgr,N is estimated at five radii. The three points at $R > 10''$ nicely overlap with the observations by M05a, showing that the two profiles are in good agreement. The two points at $R < 10''$ provide very strong new constraints on the fit of the overall profile. A $C = 1.90$ King model with $\mu_V(0) = 15.4$ and $r_c = 3.0''$ provides a good fit of the profile from the innermost observed point, at $R \simeq 3''$, to $R \sim 120'' = 2'$; for $R > 2'$ the observed profile shows a much gentler decline with respect to the model, joining the flat profile of the core of Sgr at $R = r_l \simeq 10.5'$ instead of $R = r_t \simeq 4.0'$. While there is no particular physical reason in adopting a King model to represent Sgr,N, it provides an easy and satisfying way to parametrize its inner SB profile. Moreover, while the best-fit King model fails to

[12] We used synthetic CMDs produced with the dedicated BASTI web interface (Cordier et al. 2007) to check that a population of age = 12 Gyr and [Fe/H] = −1.5 (taken as a proxy for M54) and a population of age = 6 Gyr and [Fe/H] = −0.4 (taken as a proxy for Sgr,N) having *the same total V luminosity*, places (approximately) the same number of stars in the selection windows shown in Figure 1.

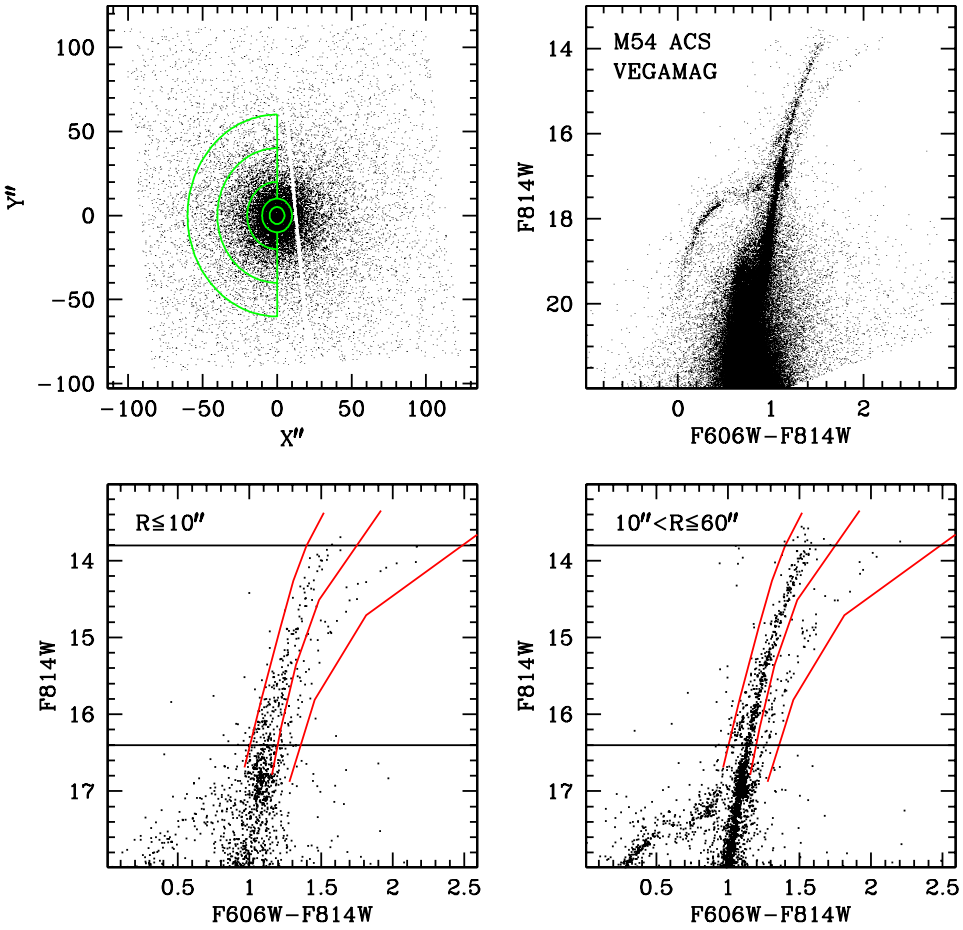

Figure 1. Upper left panel: the annuli and semi-annuli adopted for radial star counts are plotted on the X, Y map of the stars having F814W < 20.0; X, Y are the local coordinates as defined in Section 3, but in arcseconds. Upper right panel: overall CMD; note the difference among the steep and star-rich RGB of M54 and the redder and sparser RGB of Sgr,N, for F814W < 17.0. Lower panels: the selection of M54 and Sgr,N RGB stars adopted as density tracers is illustrated for two radial ranges. The horizontal lines enclose the magnitude range of the selection, the bluest and the reddest red lines select the RGB stars of both systems and the middle red line separates the sample into M54 members (bluer than the line) and Sgr,N members (redder than the line).

(A color version of this figure is available in the online journal.)

Table 2
Parameters of the King Model That Best Fits the Sgr,N Profile

Parameter	Estimate	Uncertainty	Units
r_c	0.05	±0.01	arcmin
C	1.90	...	...
r_t	4.00	±0.8	arcmin
r_h	0.42	±0.08	arcmin
r_l	≃10.5	...	arcmin
$\mu_V(0)$	15.3	±0.2	mag arcsec^{-2}
M_V	−7.8	±0.2	mag

Notes. r_t is the tidal radius of the same King model, while r_l is the observed limiting radius, defined as the radius at which the observed profile of the nucleus appears to join the profile of the overall Sgr galaxy. All the reported values and uncertainties have been estimated by assuming the reported value of C. The reported values of the SB are not corrected for interstellar extinction. r_h is the half-mass radius of the best fitting King (1966) model: it can be considered equivalent to the half-light radius, in the present case. The half-light radius of the King (1962) best fitting the SB profile of Sgr,N is $r_h = 0.23'$.

reproduce the observed profile in the range $2' \lesssim R \lesssim 10.5'$, the fraction of the total Sgr,N light enclosed in this range amounts to just a few per cent; therefore the adopted model provides a reasonable description of the distribution of the bulk of the system light.

The derived parameters are listed in Table 2. Our results are fully compatible with the limits and the educated guesses by M05a, but the most remarkable difference is in r_c which was tentatively guessed to be larger than that of M54 by M05a and, in fact, is found to be significantly smaller here. The absolute integrated V magnitude ($M_V = -7.8$) is just slightly brighter than the upper limit by M05a ($M_V \leqslant -7.6$). Assuming the best-fit models are correct, Sgr,N has a central V luminosity surface density that is slightly more than half that of M54, its total V luminosity is $\frac{1}{7}$ of the cluster and, finally both its core and half-light radii r_h are about one half of those of the cluster.[13]

[13] r_h is the half-mass radius of the best fitting King (1966) model: it can be considered equivalent to the half-light radius, in the present case. Note that using the same definition, the half-light radius of M54 is $r_h = 0.79'$, significantly larger than the value reported by Harris (1996, $r_h = 0.49'$). The latter number is very similar to what we obtain for the r_h of the King (1962) empirical model that best-fits the profile of M54 (having the same C and r_c adopted here), i.e. $r_h = 0.47'$. For $C \geqslant 1.0$ dynamical King (1966) models have r_h larger than King (1962) empirical models by more than 10%; the difference becomes larger than a factor of two for $C \geqslant 2.0$. The half-light radius of the King (1962) best fitting the SB profile of Sgr,N is $r_h = 0.23'$. Hence independently of the adopted family of models, the half-light radius of M54 is a factor of ∼2 larger than Sgr,N one. Preliminary tests suggest that available compilations of r_h likely include quantities estimated in various non-homogeneous ways.

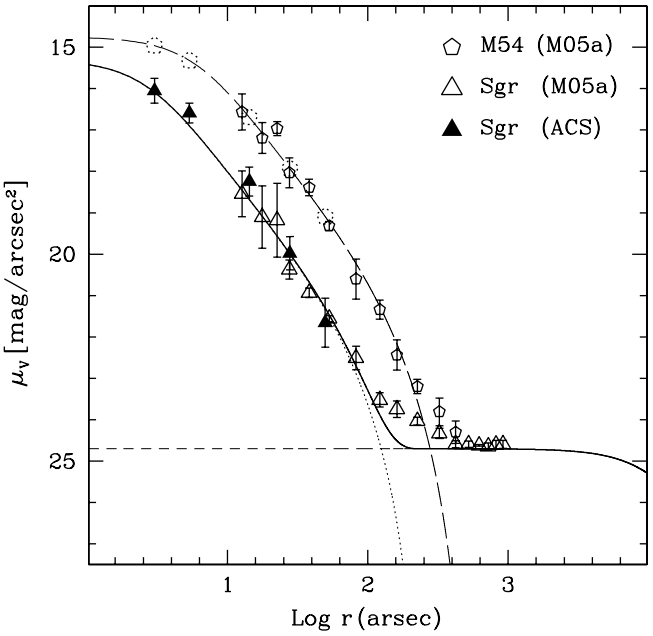

Figure 2. SB profiles of M54 (pentagons) and of Sgr (triangles). Continuous open symbols with errorbars are from M05a. The filled triangles have been obtained from the density ratio computed here from *HST*/ACS data and are normalized by adding them to the corresponding SB of the M54 best-fit model, here marked by dotted pentagons. The long-dashed line is the best-fit King (1966) model found by Trager et al. (1995) for M54; the short-dashed line is the best-fit King model found by Majewski et al. (2003) for the overall main body of the Sgr galaxy; the dotted line is the adopted best-fit model for Sgr,N and the continuous thick line is the sum of the last two models.

With these new and much tighter constraints on the light distribution of Sgr,N in hand, we will proceed in the following sections to perform a comparative study of its kinematics and those of M54.

3. THE SPECTROSCOPIC SURVEY: OBSERVATIONS, DATA REDUCTION, AND SELECTION OF THE SAMPLES

The spectroscopic observations on which this study is based were obtained with the multi-object spectrographs DEIMOS on the Keck 2 telescope and FLAMES on the VLT-UT2 telescope, as listed in Table 3. The DEIMOS observations were undertaken using two different observing strategies: the first used the standard "slitlet" mode (the slitmask approach used by the DEEP2 team, e.g., Davis et al. 2003), where short slits of minimum length 4″ and width 0.″7 were milled; the second mode used smaller 1.″5 long and 0.″7 wide "holes" to allow larger multiplexing. In both cases the high-resolution 1200 lines mm^{-1} grating was employed with the OG550 blocking filter, giving a resolution of approximately 1.4 Å FWHM. The slitlet spectra covered ∼6500–9000 Å and were extracted and wavelength calibrated using the DEEP2 pipeline software. In contrast, the "holes" spectra were extracted using software developed by our own group (Ibata et al. 2005), with the final extracted spectra covering only the region 8400–8750 Å (purely due to a limitation in the software).

For the DEIMOS observations we selected candidate M54/Sgr,N RGB and red clump (RC) stars lying within $R \lesssim 9'$ of the center of the systems from the wide-field photometry of Monaco et al. (2002). A limiting magnitude of $I = 18$ was adopted, which ensured that we probed the RGB to approximately 1 mag below the red clump (see Figure 3).

Table 3
Spectroscopic Observations

Field	Instrument	Date	Exposure
1	FLAMES Medusa 1	2005 Jul 28	3 × 845 s
2	FLAMES Medusa 1	2005 Jul 28	3 × 845 s
3	FLAMES Medusa 2	2005 Jul 28	3 × 845 s
4	FLAMES Medusa 1	2005 Aug 20	3 × 795 s
5	DEIMOS holes	2005 Aug 31	3 × 900 s
6	DEIMOS holes	2005 Aug 31	3 × 900 s
7	DEIMOS holes	2005 Oct 02	3 × 950 s
8	DEIMOS holes	2005 Oct 02	3 × 950 s
9	DEIMOS holes	2005 Oct 03	3 × 720 s
10	DEIMOS holes	2006 May 27	3 × 300 s
11	DEIMOS holes	2006 May 27	3 × 300 s
12	DEIMOS slitlets	2006 May 28	3 × 720 s
13	DEIMOS slitlets	2006 Sep 23	3 × 300 s
14	DEIMOS slitlets	2006 Sep 25	3 × 300 s

Additional FLAMES observations were downloaded from the ESO archive; these targeted almost exclusively M54 stars, with only a small contamination from other populations. The FLAMES spectra were obtained with the high resolution setting HR21, which covers the calcium triplet (CaT) from 8484–8757 Å, with a resolution of 0.5 Å FWHM. The FLAMES data were extracted and calibrated using the "girBLDRS" pipeline[14], developed for the European Southern Observatory by Geneva Observatory. Being of higher resolution, the FLAMES observations can be used to assess the accuracy of the DEIMOS data, but more importantly FLAMES is a fiber-fed spectrograph and is therefore immune to the velocity errors that can arise from mis-centering of slit spectrographs such as DEIMOS.

The radial velocities of the target stars were obtained by cross correlating the observed spectra against an artificial template of the Ca II lines, using the same approach described and discussed in detail in Ibata et al. (2005) and Battaglia et al. (2008). The determination of the uncertainty on the velocity is based on a weighted sum of Gaussian fit errors to the individual CaT lines as described in detail in the thorough discussion by Battaglia et al. (2008), who also demonstrated that the velocity errors computed in this way are reliable. An additional sanity check was provided by the comparison with the scatter of the velocity measurements derived from the three individual Ca II lines separately (see, again, Battaglia et al. 2008).

The metallicity of the target stars were estimated from the combined equivalent width of the CaT lines. To this end we implemented the calibration described by Carrera et al. (2007), which is claimed to work well up to high [Fe/H] values. As usual for CaT calibrations, [Fe/H] is a function of the combined equivalent width and of the difference between the V magnitude of the star and the mean level of the HB/RR Lyrae of the system $V - V_{HB}$. For full consistency with Carrera et al. (2007), the equivalent widths of the CaT lines were measured according to their prescriptions. The metallicity measurements were put on the Carretta & Gratton (1997) scale, assuming $V_{HB} = \langle V_{RRLy} \rangle = 18.17 \pm 0.01$ and $E(B - V) = 0.14$ (Layden & Sarajedini 2000).

3.1. Photometric Properties of the Sample

From these data we constructed a final catalogue containing the radial velocity and the metallicity of 1152 stars in the innermost $15' \times 10'$ of the Sgr galaxy, as displayed in the lower

[14] See http://girbldrs.sourceforge.net/

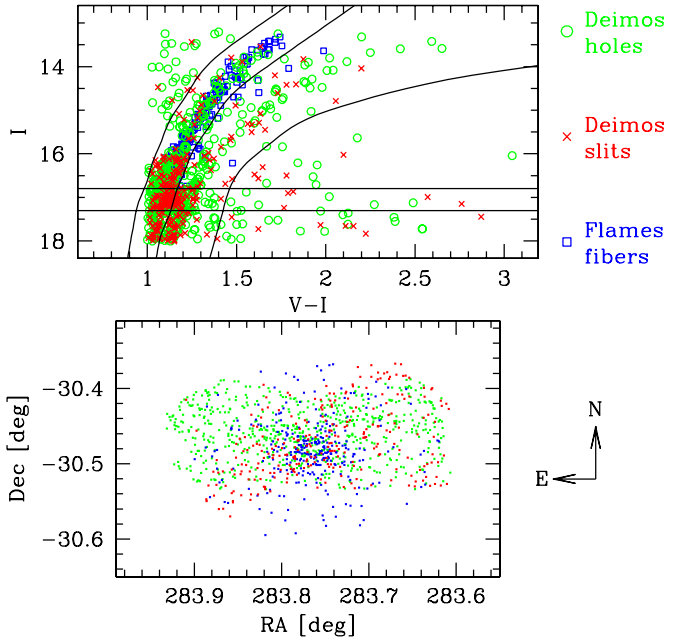

Figure 3. CMD (upper panel) and distribution in the sky (lower panel) of the 1152 stars constituting our final sample. Different colors/symbols are associated with measures obtained with different instruments and/or set-ups. The curves in the CMD show the photometric selection box adopted for a first discrimination between candidate M54 or Sgr,N members.

(A color version of this figure is available in the online journal.)

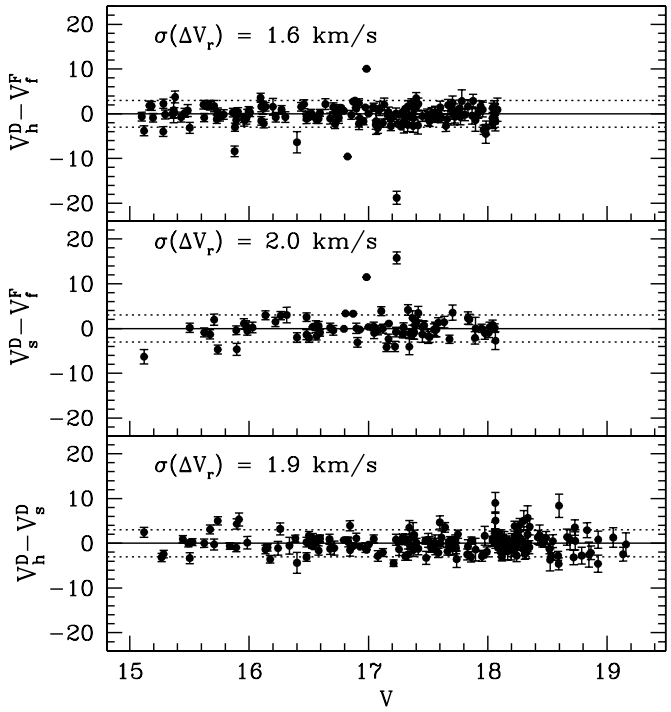

Figure 4. Comparison between independent V_r estimates obtained from spectra acquired with different telescopes/instruments/set-ups. Each panel reports the differences between the V_r estimates as a function of V magnitude. The ± 3.0 km s^{-1} range around zero is enclosed by the two dotted lines. Upper panel: DEIMOS/holes vs. FLAMES/fibers (160 stars); middle panel: DEIMOS/slits vs. FLAMES/fibers (80 stars); lower panel: DEIMOS/holes vs. DEIMOS/slits. The standard deviation of each set of ΔV_r, computed after recursive clipping of the very few 2.5σ outliers, is reported in each panel.

panel of Figure 3. The CMD of all these stars is shown in the upper panel of the same figure. The RGB sequences of the two systems are quite well separated in the CMD down to the faintest stars included in our sample ($I \simeq 18$). However, we also selected stars lying on the red clump of the Sgr,N population, at $V - I \simeq 1.15$ and $16.8 < I < 17.3$: this feature overlaps with the RGB of M54, hence we will need some further information to establish the membership of these stars, in addition to their color, magnitude, and radial velocity. In particular, the metallicity would be very useful to disentangle the two populations in this range. M54 has [Fe/H] $= -1.55$ (Brown et al. 1999; Da Costa & Armandroff 1995), with a small dispersion (see Sarajedini & Layden 1995, and Section 3.4). In contrast, the metallicity distribution of the Sgr galaxy is dominated by a wide peak at [Fe/H] $\simeq -0.4$ (see M05b; Bonifacio et al. 2006; Bellazzini et al. 2006a, and references therein), extending from [Fe/H] ~ -1.0 to [Fe/H] ~ 0.0. Stars more metal poor than [Fe/H] ~ -1.2 are quite rare and, presumably, they would pass their core-helium-burning phase as RR Lyrae or blue horizontal branch stars (Monaco et al. 2003): hence red clump stars of Sgr should have [Fe/H] $\gtrsim -1.0$, much more metal-rich than any M54 star.

As a first step for the selection of two samples representative of the Sgr,N and M54 populations, we introduced the photometric classification defined by the three curves overplotted on the CMD of Figure 3. Proceeding from left (blue) to right (red) we assigned the flag *cmd* in the following way: cmd $= 1$ to the stars enclosed between the first and second curve, as likely M54 members, cmd $= 2$ to the stars enclosed between the second and third curve, as likely Sgr,N members, and cmd $= 0$ to stars lying to the blue of the first curve or to the red of the third curve. A check *a posteriori* has shown that all the stars having cmd $= 0$ have radial velocities incompatible with being members of Sgr,N or M54, thus supporting the validity of our photometric classification.

For the coordinates of the centers of M54 and Sgr,N we adopted $\alpha_0 = 283.763750°$ and $\delta_0 = -30.478333°$ from Noyola & Gebhardt (2006), and we converted to Cartesian coordinates X, Y (in arcmin) projecting the equatorial coordinates of each star (α, δ) on the plane of sky as in van de Ven et al. (2006),

$$X = -(10800/\pi)\cos(\delta)\sin(\alpha - \alpha_0)$$

$$Y = (10800/\pi)[\sin(\delta)\cos(\delta_0) - \cos(\delta)\sin(\delta_0)\cos(\alpha - \alpha_0)],$$

with X increasing toward the west and Y increasing toward the north. Adopting the distance to Sgr and M54 measured by Monaco et al. (2004), 1 arcmin corresponds to 7.65 pc.

3.2. Comparison Between Independent Measures

As there are several stars in common between the observational sets taken with different instruments and/or set-ups, we have the opportunity to check the consistency and the accuracy of our V_r and [Fe/H] estimates. In Figure 4 we show the comparison between V_r estimates from the various sources: V_f^F are the velocities obtained with FLAMES/fibers, V_h^D are from DEIMOS/holes, and V_s^D are from DEIMOS/slits. It can be readily appreciated that the consistency among the different sets of measures is excellent (i.e., $\Delta V_r \simeq 0.0$ km s^{-1}). The typical accuracy, as measured from the rms of the V_r differences, is $\leqslant \pm 2.0$ km s^{-1}, which is satisfying for the present purpose. The actual uncertainty on the single measure should be a factor $\sqrt{2}$ smaller than the rms of ΔV_r (i.e. $\simeq \pm 1.4$ km s^{-1}), as the latter includes the uncertainties of both estimates, added in quadrature. Of the 414 velocity differences plotted in Figure 4, just $\sim$10

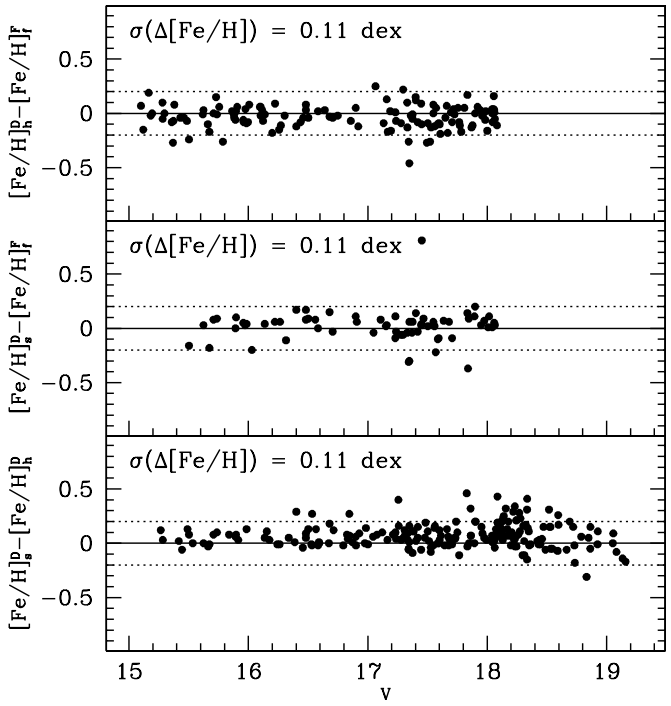

Figure 5. Comparison between independent [Fe/H] estimates obtained from spectra acquired with different telescopes/instruments/set-ups. Each panel reports the differences between the [Fe/H] estimates as a function of V magnitude. The ±0.2 dex range around zero is enclosed by the two dotted lines. Upper panel: DEIMOS/holes vs. FLAMES/fibers; middle panel: DEIMOS/slits vs. FLAMES/fibers; lower panel: DEIMOS/holes vs. DEIMOS/slits. The standard deviation of each set of Δ[Fe/H] is reported in each panel.

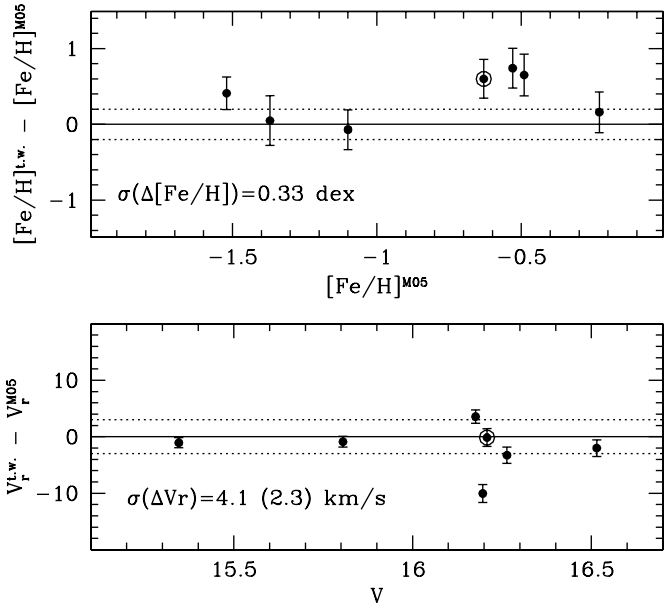

Figure 6. Comparison between the [Fe/H] and V_r estimates obtained in this work (t.w.) and M05b, for the seven stars in common. The encircled dot correspond to a star with molecular bands in its UVES spectrum, whose metallicity is classified as tentative by M05b. In the lower panel, the standard deviation value reported in parentheses refers to the sub-sample from which the outlier at $\Delta V_r \simeq 10$ km s^{-1} has been removed. The dotted lines enclose the range 0.0 ± 0.2 dex in the upper panel, and 0.0 ± 3.0 km s^{-1} in the lower panel.

are significantly larger than ±3.0 km s^{-1}: some of these may be associated with binary system observed at different orbital phases (see Monaco et al. 2007).

Figure 5 shows a comparison between [Fe/H] estimates. In this case, while the consistency between measures from FLAMES and DEIMOS/holes spectra is very good, [Fe/H] from DEIMOS/slits spectra are ∼0.08 dex larger, in average, than those from the other two sources. We were unable to find the cause of this mismatch and to preserve the homogeneity of the final merged dataset we corrected all the [Fe/H] values from DEIMOS/slits spectra by adding −0.08 to all of them. The overall accuracy is more than satisfying, with a typical rms of 0.1 dex, and also in this case the outliers are rare.

Finally Figure 6 shows a comparison between our final V_r and [Fe/H] estimates and those obtained by M05b from high-resolution FLAMES-UVES@VLT spectroscopy, for the seven stars in common between these datasets. The agreement in the radial velocity is good: if the only outlier (at $\Delta V_r \sim -10$ km s^{-1}) is excluded the rms of the difference is just 2.3 km s^{-1} and the average difference is zero.[15] Therefore the reliability and the accuracy of our radial velocity scale is fully confirmed. The comparison of metallicities is more difficult to interpret and would have benefited by a larger number of stars in common between the two samples. For four of the seven stars, ranging from [Fe/H] $\simeq -1.5$ to [Fe/H] $\simeq -0.2$ the agreement is more than acceptable, given the associated uncertainties. The other three stars show a considerable Δ[Fe/H], but one of them was reported to have a tentative [Fe/H] estimate from M05b because its spectrum was affected by molecular bands making the analysis less reliable. In any case, none of the observed differences are so large as to cause us to erroneously classify a Sgr,N star as a M54 member, or vice versa, according to the selection criteria that are adopted below. Also, taking into account the high degree of self-consistency among different sets of measures shown in Figure 5, we conclude that our metallicity scale is sufficiently reliable and accurate for the purposes of the present analysis.

3.3. Radial Velocity Distribution

The distribution of the radial velocity of all the observed stars as a function of their (projected) distance ($r = \sqrt{X^2 + Y^2}$) from the center of the system is shown in Figure 7. Two very different populations can be identified in this plot: a broadly-distributed cloud of Galactic field stars showing a large dispersion around $V_r \sim 0$ km s^{-1}, and an abundant low-dispersion population with a systemic $V_r \sim 141$ km s^{-1}, typical of M54 and Sgr,N. As a first broad selection, and following Ibata et al. (1997), we retained as possible M54/Sgr,N members all the (832) stars having 100 km s^{-1} $\leqslant V_r \leqslant$ 180 km s^{-1} (dashed lines in Figure 7). We then computed the mean and the dispersion of this sample: the ±3σ range around the global mean is enclosed within the two dotted lines. We do not reject the stars outside the 3σ range at this stage, since the velocity distribution is different at different radii (see below), and so a more refined choice is to exclude >3σ outliers in any considered radial bin. However, in Section 4 we will see that the adopted bin-by-bin 3σ rejection criterion will exclude all of these stars.

Figure 8 shows that we expect some (limited) contamination from Milky Way stars, even in our V_r selected sample. The thick continuous line superposed on the observed histogram of

[15] Also in this case we suggest multiplicity as the most likely origin of the outlier (see, again, Monaco et al. 2007). Note that binaries are not expected to significantly affect the observed velocity dispersions in systems like those considered here (see Hargreaves et al. 1996; Olszewski et al. 1996, for detailed discussion).

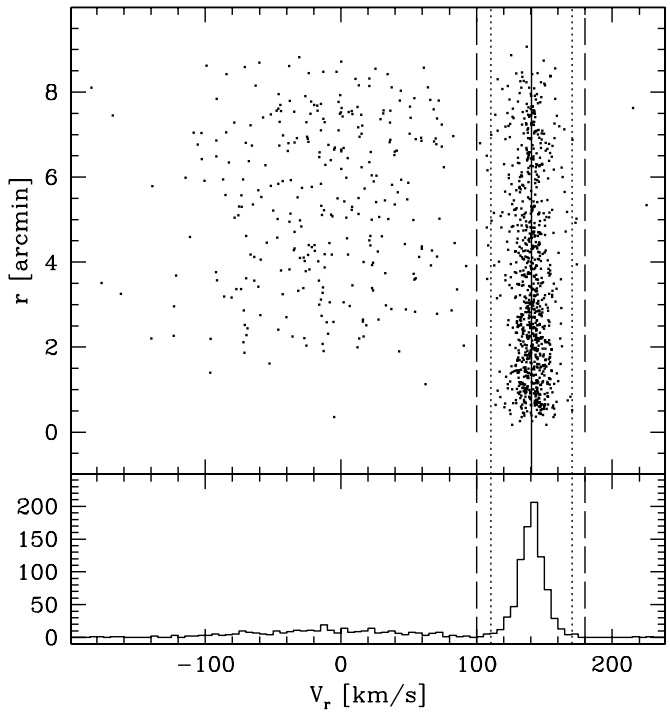

Figure 7. Radial velocity of program stars as a function of distance from the center of Sgr,N/M54 (upper panel), and radial velocity distribution (lower panel). The long-dashed lines mark the range we adopted for the first selection of candidate Sgr/M54 members. The dotted lines enclose the (global) $\pm 3\sigma$ range from the mean of the selected samples of candidates (continuous line).

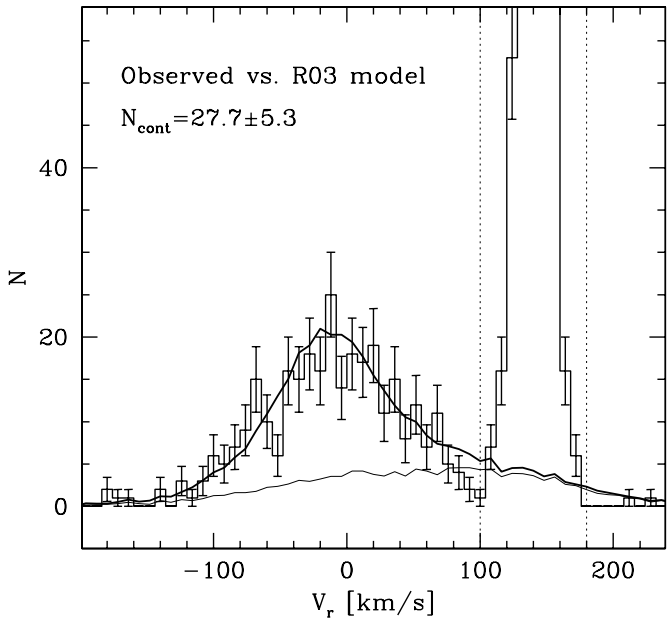

Figure 8. Zoomed view of the observed radial velocity distribution (histogram with noise error bars) around the peak of the galactic field population. The thick curve is the distribution of all galactic field stars with color and magnitude similar to program stars predicted by the R03 galactic model in the considered direction, shifted by -8 km s^{-1} to match the position of the observed peak and rescaled to minimize the χ^2 value with respect to the observations for $V_r < 100.0$ km s^{-1}. The thin curve shows the distribution of (only) giant stars from the model, with the same normalization. The vertical dotted lines enclose the 100 km s$^{-1} < V_r < 180$ km s^{-1} interval. The expected number of galactic stars falling in this velocity range $N_{\rm cont}$ is reported.

the radial velocities zoomed on the Galactic component shows the excellent agreement between the observations and the predictions of the Robin et al. (2003) Galactic model once it has been shifted by -8.0 km s^{-1} to match the observed peak and rescaled to minimize χ^2 for $V_r < 100.0$ km s^{-1}. The model suggests that up to ∼30 Milky Way stars may be present even in the relatively narrow V_r window we have adopted to select M54/Sgr,N stars. It is interesting to note that among the stars having 100 km s$^{-1} < V_r < 180$ km s^{-1} but lying outside of the $\langle V_r \rangle \pm 3\sigma$ range, seven have $V_r < \langle V_r \rangle - 3\sigma$ and four have $V_r > \langle V_r \rangle + 3\sigma$, in agreement with the trend with V_r predicted by the model. Figure 8 shows also that most of the galactic interlopers are expected to be giants, according the the Robin et al. (2003) Galactic model. However, it is likely that such stars should be, in general, much closer to us than Sgr: the model finds that the contaminating giants have a mean distance of 8.7 kpc (corresponding to $\Delta(M - m) = +2.4$ mag, with respect to Sgr), 90% of them have $D \leqslant 11$ kpc and 99% of them have $D \leqslant 14$ kpc, i.e. much lower than $D_{\rm Sgr} = 26.3$ kpc. For this reason the difference between their V magnitude and $V_{\rm HB}$ of Sgr must be a bad proxy for their gravity. The typical spectroscopic metallicity error incurred by overestimating the distance modulus of these galactic stars by 2.4 mag is Δ[Fe/H] $= -0.58$, so the stars will appear to be less metal-rich than they are in reality while their color and magnitude mimic those of genuine Sgr/M54 stars. As a consequence, the metallicity obtained for a galactic star from the calcium triplet (CaT) technique would normally be much different from what would be expected from the magnitude and color measurements. Therefore, there is some hope to exclude these galactic interlopers from our final samples, identifying them by their "odd" color—metallicity combination, as we will do in our final selection (Section 3.5). As the mean metallicity of contaminating giants is $\langle$[Fe/H]$\rangle = -0.75$ and 90% of them have [Fe/H] < -0.33 it is quite likely that many of them would have a measured metallicity lower than the lower threshold we will assume for Sgr,N members ([Fe/H] $\geqslant -0.8$). On the other hand, those spuriously showing metallicities compatible with M54 will probably be too red to be selected as possible cluster members (Section 3.5 and Figure 3).

Finally it is worth noting that the spectra of all the 843 stars that passed the selection in V_r have signal-to-noise ratio (per pixel) S/N > 12; 300 of them have S/N > 50 and 63 of them have S/N > 100 (see Figure 9(d)).

3.4. Metallicity Distribution

The metallicity distribution of the velocity selected stars is shown if Figure 9(a). The presence of two populations is very clear: there is a metal-poor peak around [Fe/H] $\simeq -1.5$ that must be dominated by M54 stars (Brown et al. 1999) and a broader distribution extending from [Fe/H] $\gtrsim -1.0$ to super-solar metallicity corresponding to the main population of Sgr,N (see M05b; Bellazzini et al. 2006a; Bonifacio et al. 2006, and references therein). As mentioned earlier, in the present context we will use the metallicity just as a further means to select samples of M54 and Sgr,N members that are as clean as possible, so as to allow further analysis of their kinematic properties. Therefore, we limit the discussion of the metallicity to the brief considerations listed below.

1. We confirm that the bulk of Sgr stars have [Fe/H] > -1.0, belonging to a broad distribution peaking around [Fe/H] $= -0.4$ and reaching super-solar metallicities (M05b; Bonifacio et al. 2006). Monaco et al. (2003) estimated that in the main body of the Sgr galaxy old

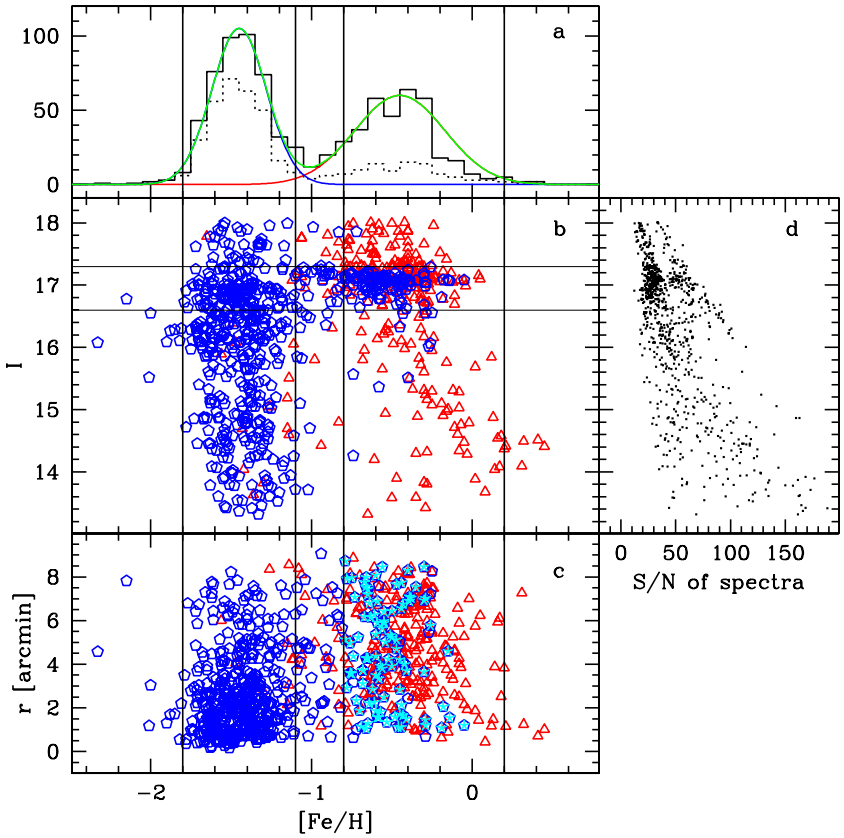

Figure 9. Selection of clean samples of M54 and Sgr,N members. Panel (a): metallicity distribution of the 843 stars that survived the selection in radial velocity. The superposed curve is the sum of two Gaussian distributions having mean and standard deviation $(\langle[Fe/H]\rangle, \sigma) = (-0.45, 0.28)$ and $(-1.45, 0.17)$, representing the main populations of Sgr,N and M54, respectively. The dotted histogram is the observed distribution for stars having $R \leqslant 3.0'$. Panel (b): metallicity vs. I magnitude; open triangles are stars having cmd = 2, i.e. photometrically selected as likely Sgr members (see Figure 3); open pentagons are stars with cmd = 1, i.e. photometrically selected as likely M54 members. The horizontal lines enclose the Sgr RC magnitude range ($16.6 < I < 17.3$). The vertical lines mark the adopted thresholds in metallicity: $-1.8 \leqslant$ [Fe/H] $\leqslant -1.1$, for the M54 sample; $-0.8 \leqslant$ Fe/H] $\leqslant +0.2$ for the Sgr,N sample. Panel (c): metallicity vs. distance from the center of M54. The symbols are the same as in the above panel, except for asterisks superposed on open pentagons: these are stars that lie on the RGB of M54 in the CMD but in fact belong to the superposed RC of Sgr, i.e., they have $16.6 < I < 17.3$ and a metallicity typical of Sgr members. Panel (d): S/N (per pixel) of the spectra as a function of I magnitude. All the spectra have S/N > 12.

(A color version of this figure is available in the online journal.)

metal-poor stars ([Fe/H] $\lesssim -1.2$) should provide less than 12% of the whole stellar content. Several arguments suggest that this fraction should be even lower in the very central region considered here (see Alard 2001; Bellazzini et al. 2006b; Siegel et al. 2007, and references therein). However, we note that there are four stars having [Fe/H] < -2.0 in our sample (see Figure 9) that are probably too metal poor to be members of M54 and might be part of the metal-poor population of Sgr.

2. The peak of the metallicity distribution corresponding to M54 is best fitted by a Gaussian curve having mean $\langle[Fe/H]\rangle = -1.45$. This is slightly higher ($\sim$+0.1) than what was found by Brown et al. (1999) and by Da Costa & Armandroff (1995), while it is in good agreement with Armandroff (1989). Note that any possible small shift in the zero point of our metallicity scale does not affect the accuracy of the metallicity *ranking*, that is $\simeq \pm 0.1$ and it is the relevant figure in the present context.

3. Based on the analysis of the color—magnitude distribution of RGB stars, Sarajedini & Layden (1995) concluded that there is an intrinsic metallicity spread among M54 stars of $\sigma_{\rm int}([Fe/H]) = 0.16$ dex. Using spectroscopic metallicities obtained with the CaT technique for five M54 members, Da Costa & Armandroff (1995) found further support for this hypothesis (but see Brown et al. 1999).[16] Our much larger sample of CaT metallicities provides new supporting evidence for this possibility. The sample with $-1.0 \leqslant$ [Fe/H] $\leqslant -2.0$ has an observed standard deviation of 0.17 dex, larger than what is expected from the statistical scatter (see Figure 5). Deconvolving the (internal) rms scatter (0.11 dex, see Figure 5) from the observed width of the distribution we obtain an estimate of the intrinsic spread of $\sigma_{\rm int}([Fe/H]) = 0.14$ dex, in good agreement with previous estimates. It seems very unlikely that the width of the M54 peak is significantly contaminated by Sgr stars, as the width remains unchanged if we limit the sample to the innermost 3′ where M54 should dominate the population mix. If finally confirmed by high-resolution spectroscopy of a large sample of stars, the purported metallicity spread would constitute another element of similarity between M54 and other large-size very bright clusters such as ω Cen, G1 and the like, which are also suspected of being remnant nuclei of disrupted galaxies (see Mackey & van den Bergh

[16] G. Wallerstain kindly pointed out in a private communication to M.B. that in Brown et al. (1999) it was explicitly stated that the sample considered in that analysis was not sufficient to establish or exclude the presence of a metallicity spread in M54.

2005; Federici et al. 2007; Catelan 2008; Maschenko & Sills 2005; Böker 2008, and references therein).

We think that the currently available metallicity estimates provide a metallicity ranking that is more than sufficient for the purposes of the present paper, i.e., (a) to discriminate M54 stars from Sgr,N stars in the magnitude range where the two population overlaps in the CMD ($16.8 < I < 17.3$), and (b) to exclude possible interlopers as stars having the "wrong" metallicity for their color. The details of the adopted selections are described in the following subsection.

3.5. The Final Selections

The scheme of our finally adopted selections is illustrated in Figures 9(b) and (c). Our aim is to have a sample of M54 stars and a sample of Sgr,N stars as clean as possible from any kind of interlopers. The adopted criteria are the following:

1. We accept as members of the M54 sample the stars having cmd = 1 and $-1.8 \leqslant$ [Fe/H] < -1.1.
2. We accept as members of the Sgr,N sample the stars having cmd = 2 and $-0.8 \leqslant$ [Fe/H] $\leqslant +0.2$, or having cmd = 1 and $-0.8 \leqslant$ [Fe/H] $\leqslant +0.2$ if $16.6 < I < 17.3$ (Sgr RC stars superposed on the RGB of M54).

The metallicity separation avoids mixing between samples. The requirement that the cmd flag and the metallicity broadly agree in assigning the membership is likely to exclude most of the Galactic interlopers. In the region in which the RC of Sgr,N and the RGB of M54 overlap, the cmd flag does not provide any discrimination and we rely just on the metallicity. We have adopted quite conservative criteria to obtain very reliable samples of genuine Sgr,N and M54 stars. As a further check, all the results presented in the following about the kinematics of Sgr,N have been verified to hold also when subsamples in which stars in the RC region were excluded are adopted. The main properties of the selected samples are shown in Figure 10.

With the selection described above we select a sample of 425 very likely M54 members and of 321 very likely Sgr,N members. In the process of clipping 3σ velocity outliers in any considered radial bin (which will be performed in Section 4), we will further exclude eight stars from the M54 sample and three stars from the Sgr,N sample. Hence the actual detailed analysis of the kinematics of the two systems will be performed on 417 stars for M54 and on 318 stars for Sgr,N.

4. THE KINEMATICS OF M54 AND Sgr,N: OBSERVATIONAL FACTS

In Table 4 we list the estimates of some relevant physical parameters of M54 that are available in the literature. For the structural parameters (r_c, r_t, etc) we will preferentially adopt those from Trager et al. (1995), since the best-fit model proposed by these authors is in good agreement with the profile obtained from star counts in the outer regions of the cluster by M05a. However, in some cases we will consider the effects of the adoption of different sets of parameters on our results. It is reassuring that most authors derived quite similar parameters from very different datasets. All the available mass estimates for M54, also obtained with different methods and from different datasets, range between $1.0 \times 10^6\,M_\odot$ and $2.0 \times 10^6\,M_\odot$ (Illingworth 1976; Mandushev et al. 1991; Pryor & Meylan 1993; Mackey & Gilmore 2003; McLaughlin & van der Marel 2005).

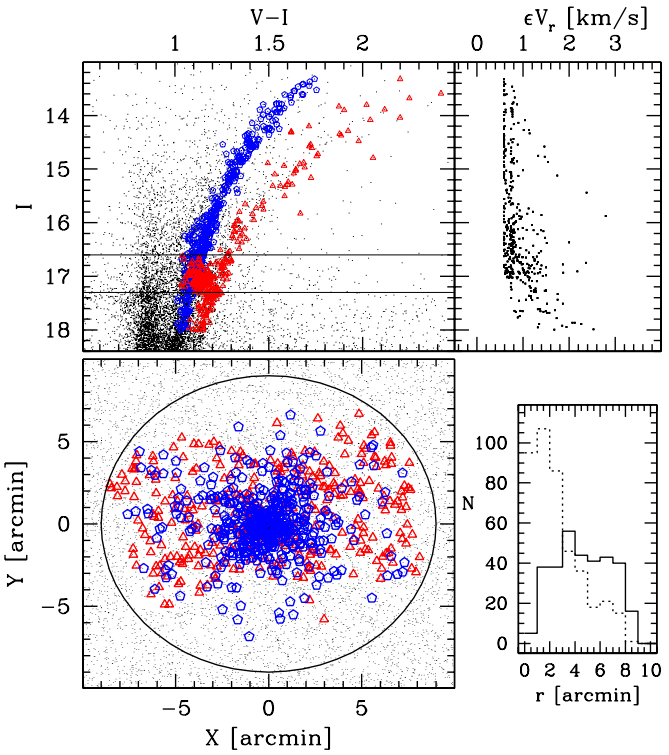

Figure 10. Upper left panel: CMD of stars selected to belong to the final Sgr,N (open triangles) and M54 (open pentagons) samples, superposed on the CMD of all stars having $R < 9'$ from Monaco et al. (2002, small dots). The thin horizontal lines enclose the red clump of Sgr ($16.6 < I < 17.3$). The position in the sky of the selected stars relative to the center of Sgr,N/M54 is plotted in the lower left panel, the symbols are the same as above. The radial distributions of stars selected on the Sgr,N sequences (continuous histogram) and on the M54 sequences (dotted line) are plotted in the lower right panel. The upper right panel shows the uncertainties of the V_r estimates as a function of I magnitudes for the selected stars.

(A color version of this figure is available in the online journal.)

In Table 5 we report the average kinematical properties of the M54 and Sgr,N samples as a whole. The errors on all the reported quantities have been obtained by a jackknife bootstrapping technique (Lupton 1993). The plain average V_r of the two samples differs by 1.5 ± 0.7 km s^{-1}, that is, just a $\sim 2\sigma$ difference. However, an average with iterative 2σ clipping seems a much more appropriate estimator of the systemic velocity since it is very robust to outliers and is more effective in estimating the mode of the samples. The sigma clipping process converges very fast in both cases, leaving very rich final samples ($N_{2\sigma} = 246$ and 348, for Sgr,N and M54, respectively). The difference in the clipped mean velocities is a mere 0.8 km s^{-1}. We conclude that the Sgr,N and M54 do coincide also in line-of-sight (LOS) velocity, a further proof in support of their spatial coincidence. Many authors have noted previously that the systemic velocity of Sgr and M54 are very similar (Ibata et al. 1997; Da Costa & Armandroff 1995; M05b); we think we have conclusively established here that M54 and the nucleus of Sgr have the same systemic LOS velocity, within $\simeq \pm 1.0$ km s^{-1}.

The velocity dispersions of the whole Sgr,N and M54 do not seem very different, at a first glance. However, it should be recalled here that in the radial range covered by our data ($r \leqslant 9'$), the SB of M54 and Sgr,N declines by more than ~ 8 mag arcsec^{-2}. Hence, in the present context, what is really relevant is the comparison between velocity dispersion profiles

Table 4
Literature Data for M54

r_c (arcmin)	r_t (arcmin)	C	$\mu_V(0)$ (mag arcsec^{-2})	V_t (mag)	[Fe/H] (dex)	Method	References
0.11	7.4	1.83	14.90	7.61		g.b. ap. phot.	Illingworth & Illingworth (1976)
				7.68		g.b. ap. phot.	Peterson (1993)
0.11	7.4	1.84	14.75			g.b. ap. phot.	Trager et al. (1995)
					−1.55	CaT spectr.	Da Costa & Armandroff (1995)
					−1.55	HR spectr.	Brown et al. (1999)
$\lesssim$0.11						*HST* phot.	Mackey & Gilmore (2003)
0.09	9.9	2.04	14.35			g.b. ap. phot.	McLaughlin & van der Marel (2005)
0.05			14.12			*HST* phot.	Noyola & Gebhardt (2006)

Notes. g.b. ap. phot. = ground based aperture photometry; *HST* phot. = integrated photometry and/or star counts from *HST* data; CaT spectr. = medium resolution spectroscopy using the infrared calcium triplet as metallicity indicator; HR spectr. = High Resolution spectroscopy and elemental abundance analysis. See also Webbink (1985), Harris (1996), and Mackey & Gilmore (2003) for collections of literature data on M54.

Table 5
Average Kinematic Properties of the M54 and Sgr,N Samples

	$N_{\rm tot}$	$\langle V_r\rangle$ (km s^{-1})	σ (km s^{-1})	σ^* (km s^{-1})	$N_{2\sigma}$	$\langle V_r\rangle_{2\sigma}$ (km s^{-1})
Sgr,N	321	139.4 ± 0.6	10.0 ± 0.5	9.6 ± 0.4	246	139.9
M54	425	140.9 ± 0.4	9.3 ± 0.5	8.3 ± 0.3	348	140.7

Notes. $N_{2\sigma}$ = number of stars in the sample once the iterative 2σ clipping algorithm to compute $\langle V_r\rangle_{2\sigma}$ has converged, i.e., there is no more 2σ outlier. Note that at each iteration the algorithm adopts the *current* value of 2σ that is, in general, significantly lower than the *global* value reported in the table. σ^* are the global values of the dispersion after the exclusion of the local $>3\sigma$ outliers performed in Section 4.1. They are computed from the final cleaned samples of 318 (Sgr,N) and 417 (M54) stars, as already reported in Section 3.5.

as a function of distance from the center of the system, which will be presented in the following section.

4.1. Velocity Dispersion Profiles

In the upper panel of Figure 11 we show the distribution of the M54 stars in the V_r versus r plane. We have divided the sample into two sets of six and five independent radial bins of different size, respectively, in order to keep the number of stars per bin as high as possible while maintaining the highest degree of spatial resolution (the primary set of independent bins corresponds to the odd rows of Table 6, the secondary set corresponds to the even rows of the table). The primary bins are enclosed by the vertical lines. In each bin we computed the average V_r and the velocity dispersion σ, with their uncertainties (derived with the "jackknife" method, as above). An iterative 3σ clipping algorithm was applied bin by bin. As we proceeded from the innermost bin to the outer ones, any star rejected in a given bin by the clipping algorithm was excluded from the sample. The eight rejected stars are clearly indicated in the plot.

The derived velocity dispersion profile is reported in the lower panel of Figure 11 (large filled pentagons, primary set, small filled pentagons, secondary set) and in Table 6. The table reports also an alternative estimate of σ obtained with the Gaussian maximum-likelihood method described by Walker et al. (2006), essentially equivalent to that adopted by Martin et al. (2007). It is remarkable that in all cases the estimates obtained with the two methods differ by much less than the reported uncertainties (in all cases by $\leqslant$0.3 km s^{-1}). The profile is complemented with the central estimate obtained by Illingworth (1976) from integrated spectroscopy of the cluster core.[17] The profile shows a steep decrease from $\sigma = 14.2$ km s^{-1} at the center to $\sigma \simeq 5.0$ km s^{-1} at $r = 3\farcm5$. Then it begins to grow gently up to $\sigma \simeq 9$ km s^{-1} in the last bin ($r \simeq 7'$).

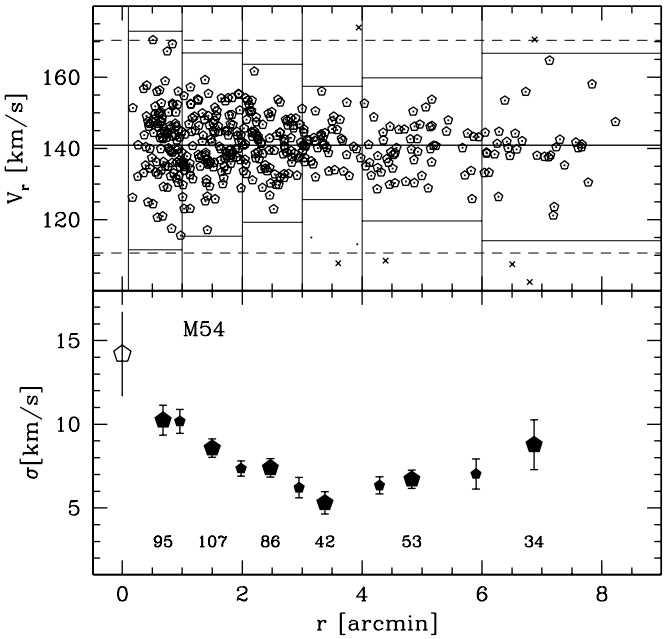

Figure 11. Velocity dispersion profile of M54 stars. The upper panel shows the V_r distribution as a function of distance from the cluster center for individual stars of the M54 sample. Only stars plotted as dots encircled by open pentagons are retained for the computation of σ in the various radial bins: small dots alone are stars rejected only because they are "local" 3σ outliers of the bins, crosses are stars that would have been rejected also as 3σ outliers of the whole Sgr,N + M54 sample (the global $\pm 3\sigma$ range is enclosed by the long-dashed lines). The vertical lines display the adopted independent bins, of variable size. The global mean is marked by the continuous horizontal thick line. The lower panel displays the actual velocity dispersion profile. The large filled pentagons are the dispersions estimated in the corresponding bins displayed in the upper panel, with their bootstrapped errors. The number of stars per bin is also reported below the points. The small filled pentagons are the estimates in the additional, partially overlapping, bins. The open pentagon is the estimate of σ at the center of M54 obtained by Illingworth (1976) from integrated spectroscopy.

Figure 12 shows the velocity distribution and dispersion profile for the Sgr,N sample, with the same arrangement as

[17] Here we adopt the estimate of central velocity dispersion $\sigma_0 = 14.2$ km s^{-1} obtained by Illingworth by correcting the value he measured from integrated long-slit spectroscopy of the cluster center.

Table 6
Velocity Dispersion Profile for M54

r_i (arcmin)	r_f (arcmin)	r_m (arcmin)	σ (km s^{-1})	e_σ (km s^{-1})	σ_{ml} (km s^{-1})	e_σ (km s^{-1})	N
0.1	1.0	0.68	10.2	0.9	10.1	1.0	95
0.5	1.5	0.96	10.2	0.7	10.1	1.1	131
1.0	2.0	1.50	8.6	0.5	8.5	1.2	107
1.5	2.5	1.98	7.4	0.4	7.2	1.4	101
2.0	3.0	2.47	7.4	0.5	7.3	1.3	86
2.5	3.5	2.95	6.2	0.6	6.1	1.3	66
3.0	4.0	3.38	5.3	0.7	5.1	1.2	42
3.5	5.0	4.29	6.3	0.5	6.2	1.1	49
4.0	6.0	4.83	6.7	0.5	6.6	1.1	53
5.0	7.0	5.89	7.0	0.9	6.9	0.9	36
6.0	9.0	6.87	8.8	1.5	8.6	0.7	34

Notes. r_i and r_f are the limits of the bins, r_m is the radius of the middle of the bins. N is the number of stars in the bin, after the rejection of 3σ outliers. σ_{ml} is the velocity dispersion estimated with a Gaussian *maximum likelihood* method as done in Walker et al. (2006).

Table 7
Velocity Dispersion Profile for Sgr,N

r_i (arcmin)	r_f (arcmin)	r_m (arcmin)	σ (km s^{-1})	e_σ (km s^{-1})	σ_{ml} (km s^{-1})	e_σ (km s^{-1})	N
0.8	2.0	1.41	9.1	0.9	8.9	0.7	41
2.0	3.0	2.55	8.8	1.2	8.6	0.7	38
3.0	4.0	3.54	10.2	0.9	10.0	0.7	56
4.0	5.0	4.47	8.8	1.0	8.5	0.9	43
5.0	6.0	5.46	9.6	1.1	9.3	0.7	40
6.0	7.0	6.52	8.7	0.9	8.5	0.7	43
7.0	9.0	7.69	10.3	1.1	10.1	0.7	56

Notes. r_i and r_f are the limits of the bins, r_m is the radius of the middle of the bins. N is the number of stars in the bin, after the rejection of 3σ outliers. σ_{ml} is the velocity dispersion estimated with a Gaussian *maximum likelihood* method as done in Walker et al. (2006).

in Figure 11 (see also Table 2). The absence of any obvious trend of velocity dispersion with radius allowed us to adopt a single set of bins of nearly uniform size. The dispersion in each bin has been estimated exactly as in the case of M54, described above. The two innermost stars of the sample (crosses) have been excluded from the analysis as they lie in a too poorly sampled radial region ($r < 0.8'$) and may affect the computation of the mean radius of the first bin. However, the inclusion of these stars in the innermost bin changes the velocity dispersion estimate by $\simeq$0.2 km s^{-1}.

It is quite obvious from the inspection of Figure 12 that the velocity dispersion profile of Sgr,N is completely flat over the whole radial range explored by our data. The lower panel shows that the velocity dispersion of each radial bin is in good agreement with the velocity dispersion of the whole sample after the clipping of 3σ outliers, $\sigma = 9.6 \pm 0.4$ km s^{-1}. The maximum observed difference among bins is 1.6 ± 1.4 km s^{-1}; the maximum difference between the dispersion in a given bin and the dispersion of the whole sample is -0.9 ± 1.0. Possibly, there may even be a weak tendency toward lower-velocity dispersions in the inner regions: in the range $0\farcm0 \leqslant r < 5\farcm0$ we find $\sigma = 9.2 \pm 0.5$ km s^{-1} (180 stars), while in the range $5\farcm0 \leqslant r < 9\farcm0$ we find $\sigma = 10.1 \pm 0.6$ km s^{-1} (138 stars); however, this difference is clearly not statistically significant (see Geha et al. 2002; Valluri et al. 2005, for some example of the variety of velocity dispersion profiles observed in dE,N).

It is rather clear that the nucleus of Sgr and the M54 cluster have different velocity dispersion profiles. M54 displays the typical behavior of a globular cluster, i.e., the system becomes increasingly kinematically hot toward its central regions while Sgr,N has a uniformly flat profile, though the SB profiles of the two systems are broadly similar. Figure 13 shows a comparison between the profiles in deeper detail. The inner growth of σ of M54 stars makes the two profiles overlap at $r \sim 1.5'$; the innermost two points of the M54 profile are hotter than any Sgr,N point. The outermost point of the cluster profile does match the dispersion of Sgr,N: the velocity dispersion estimate here comes from the least populated bin as well as the most (possibly) prone to contamination by old and metal-poor stars belonging to Sgr (see below for a more detailed discussion). These are the reasons why the comparison between the two samples taken as a whole does not reveal any striking difference. However, in the intermediate radial range the M54 population is significantly colder than that of Sgr,N and the statistical significance of this result is *very strong*.

Table 8 reports the results of non-parametric Kolmogorov–Smirnov tests performed on different radial ranges. In all the considered ranges the probability that the two samples are drawn from the same parent population is smaller than 2% and it is smaller than 0.2% in the $1.5' \leqslant r < 6.5'$ range. In the present case, however, the F statistic is the most appropriate mean to compare statistically the two samples ($F = \sigma^2_{\rm Sgr}/\sigma^2_{\rm M54}$, see Brandt 1970, and references therein), as the corresponding F test evaluates the probability that two samples of given F value are extracted from Gaussian distributions having the same σ. Table 9 shows that in our case this probability is lower than 0.3% in all

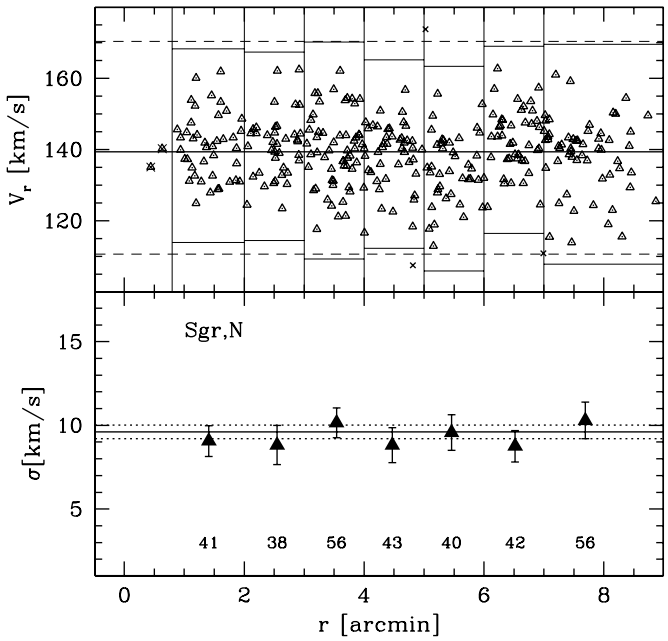

Figure 12. The same as Figure 11 for the Sgr,N sample (triangles replace pentagons here). The two innermost point are rejected for reasons of uniformity of the sample. In the lower panel we also report the velocity dispersion of the whole sample as a continuous line, ± the associated error (dotted lines). As σ does not appear to change with radius we use only the reported seven independent bins.

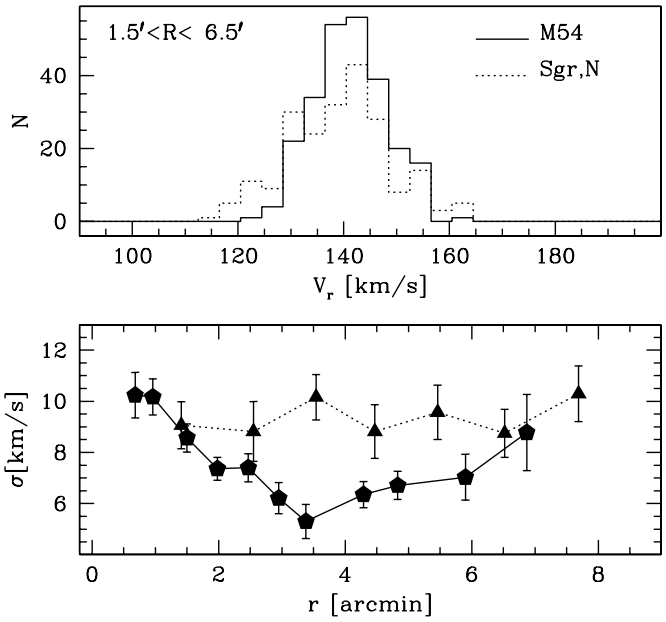

Figure 13. Upper panel: Velocity distribution of the M54 and Sgr,N samples in the radial range in which the difference in their σ reaches the maximum statistical significance, according to the F test (see Table 9. Lower panel: comparison of the velocity dispersion profiles of M54 (continuous line and pentagons) and Sgr,N (dotted line and triangles).

Table 8
KS Test: Probability That the Sgr,N and the M54 Samples Are Drawn from the Same Parent Population

r_i	r_f	N_{M54}	$N_{Sgr,N}$	D_{KS}	P%
0.0	9.0	417	318	1.649	0.87
0.8	8.0	353	300	1.531	1.84
2.0	7.0	199	219	1.624	1.02
2.0	6.0	181	177	1.698	0.63
1.5	6.5	247	213	1.817	0.13

Notes. KS = Kolmogorov–Smirnov. r_i and r_f are the limits of the considered radial ranges, N_{sample} is the number of stars of the sample in the considered radial range. 3σ outliers have been excluded from the samples.

the considered radial range and it is as small as $< 0.01\%$ in several intermediate ranges, including $1.5' \leqslant r < 6.5'$. While such a large quantitative difference may not be so obviously apparent from the dispersion profile, it is clear at a first glance when looking at the comparisons in the X–V_r and in the R–V_r planes shown in Figure 14.

Hence, the direct comparison of the velocity distributions of the two samples clearly establishes that the two populations have very different kinematic properties, indicating that the motion of M54 stars and that of Sgr,N stars are driven by different gravitational equilibria.

Moreover, Gilmore et al. (2007) clearly states that a velocity dispersion profile monotonically declining from the center outward "...is an unavoidable requirement for any mass-follows-light system..." In the present case, this means that while M54 behaves like an ordinary mass-follows-light "purely baryonic" self-gravitating star cluster (at least in its innermost region, containing most of its light/mass; see also Figure 14 and Section 4.2), the flat velocity dispersion profile of Sgr,N implies that the mass distribution driving the kinematics of the nucleus is significantly different from the distribution of the stars. In principle, a radial gradient in the velocity anisotropy affecting only one of the two systems may be invoked to explain the observed difference in the velocity dispersion profiles. As this would imply a correlation of the anisotropy variation with metallicity, we regard this hypothesis as rather *ad hoc* and we no longer discuss it in the following. We will re-consider the case in more detail in a future contribution (R. A. Ibata et al. 2008, in preparation).

Finally, the velocity dispersion profile of Sgr,N does not differ significantly from the overall profile of the Sgr galaxy, which is found to be flat out to large radii (Ibata et al. 1997), as typical of dwarf spheroidals (see Walker et al. 2006; Muñoz et al. 2008, and references therein). In Figure 15 we have combined the inner $0.8' \leqslant r \leqslant 9'$ profile obtained here, with estimates of the dispersion at different radii out to $r \simeq 100'$ obtained from publicly available data from the literature (M05b; Ibata et al. 1997) in the same way as done for M54 and Sgr,N, above. Note that $r \simeq 100'$ is less than half of the core radius of the whole Sgr galaxy (Majewski et al. 2003). All the observations are consistent with a constant σ in the considered range and, in particular, there is no apparent transition in the profile at the onset of the nuclear overdensity of stars ($r \leqslant 10'$). This fact strongly suggests that the inner kinematics of Sgr, including its nucleus, is dominated by the potential set by a distribution of unseen (dark) matter, not by M54 as in the scenario (b) described in Section 1.

4.2. Comparison with Models

In Figure 16 the observed velocity dispersion profile of M54 is compared with the theoretical profiles of single-mass isotropic King (1966) models that have been proposed by various authors as best-fits to the SB profile of the cluster (see Table 4). The models proposed by Trager et al. (1995, continuous line) and

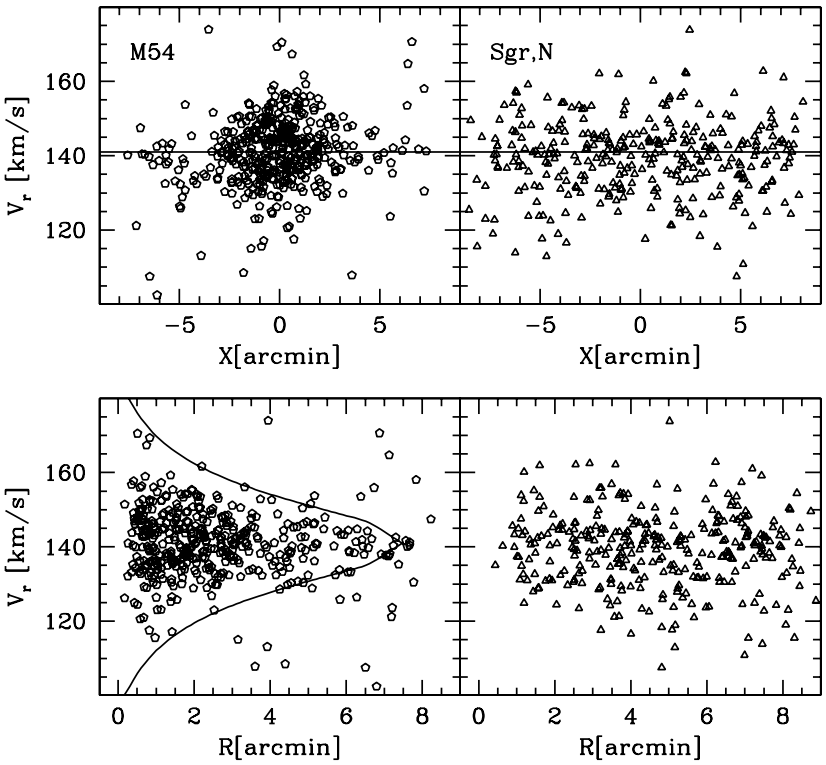

Figure 14. Direct comparison of the velocity and spatial distributions of M54 and Sgr,N. Upper panels: V_r as a function of X for the M54 (left panel) and for the Sgr,N (right panel) samples. Lower panels: V_r as a function of R for the same samples. The curves in the lower left panel are the $\pm 3\sigma$ profiles the best-fit King model for M54 (Trager et al. 1995), approximately representing the envelope of the allowed velocities for bound members of M54.

Table 9
F Test: Probability That the Sgr,N and the M54 Samples Are Drawn From Gaussian Distributions Having the Same σ

r_i	r_f	N_{M54}	$N_{Sgr,N}$	F	P%
0.0	9.0	417	318	1.345	0.23
0.8	8.0	353	300	1.448	0.04
2.0	7.0	199	219	2.010	<0.01
2.0	6.0	181	177	2.019	<0.01
1.5	6.5	247	213	1.978	<0.01
2.5	3.5	65	51	2.546	0.02
1.5	3.5	166	80	1.862	0.04

Notes. r_i and r_f are the limits of the considered radial ranges, N_{sample} is the number of stars of the sample in the considered radial range. 3σ outliers have been excluded from the samples. F is computed as $F = \sigma^2_{Sgr,N}/\sigma^2_{M54}$.

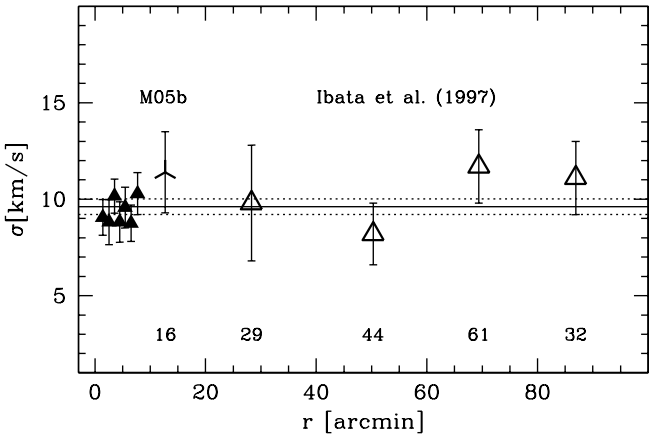

Figure 15. Velocity dispersion profile of the innermost $\sim 100'$ of the Sgr galaxy. Filled triangles are the $r < 10'$ estimates obtained here, the skeletal symbol is from the M05b stars having [Fe/H] < -1.0 (to avoid possible M54 members), open triangles are from Table 2b of Ibata et al. (1997) (CTIO-ARGUS radial velocities). The horizontal lines are the same as in Figure 12. Note that this composite profile covers less than half of the core radius of the Sgr galaxy ($r_c \simeq 220'$ Majewski et al. 2003).

by McLaughlin & van der Marel (2005, dashed line) provide a reasonable description of the data out to $r \lesssim 4'$, while there is a clear tendency of the data to be hotter than the models for $r > 4'$. The outermost observed point, at $r \simeq 7' \lesssim r_t$, displays a velocity dispersion significantly higher than what is predicted even by the hottest model $[\sigma_{obs} - \sigma_{KM}]_{r\sim 7'} = 5.8 \pm 2.0$ km s^{-1}. There are two possible explanations for this unexpected rise of the velocity dispersion curve near the tidal radius of the cluster.

First, while our selection criteria prevents any contamination of the Sgr,N sample by M54 stars, since cluster stars with [Fe/H] $\geqslant -0.8$ simply do not exist, it is well known that the Sgr galaxy does host a minority of stars with [Fe/H] $\leqslant -1.0$ ($\lesssim$12%, Monaco et al. 2003), hence some degree of contamination of the M54 sample by Sgr stars is expected (see Section 3.1) and the less populated outer bins of the M54 profile are clearly the most sensitive to the effect of the inclusion of contaminants. Rough estimates indicate that the contamination by metal-poor Sgr stars should amount to less than 3% in the innermost $2'$, less than 10% for $2' \leqslant r < 4'$, but it can raise to $\lesssim 20\%$ for $4' \leqslant r < 6'$ and be even larger for $r > 6'$. So, contamination by metal-poor Sgr stars seems a viable explanation for the rise of the dispersion profile of M54 such that it becomes similar to that of the Sgr,N sample in the outermost, and presumably most contaminated, bin.

Alternatively, it may be conceived that, during its spiraling toward the center of Sgr,N (see Section 5.2), M54 suffered

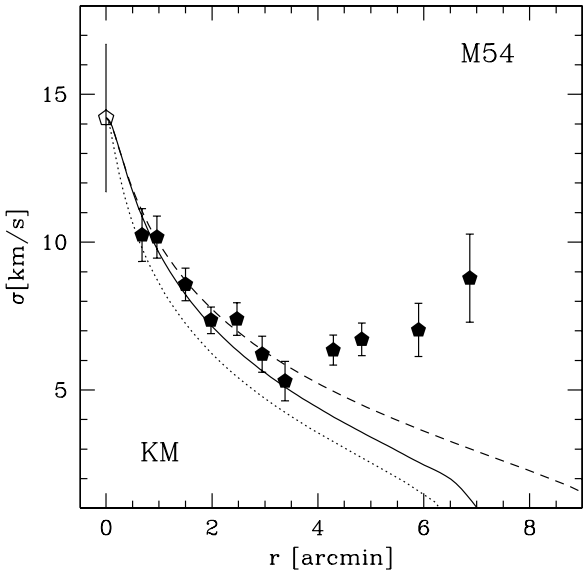

Figure 16. Comparison of the observed velocity dispersion profile of M54 with King models that best fit the SB profile of the cluster, as proposed by various authors (see Table 4), and normalized to $\sigma_0 = 14.2$ km s^{-1}. Continuous line: $r_c = 0.11'$ and $C = 1.85$, from Trager et al. (1995). Dotted line: $r_c = 0.053'$ from Noyola & Gebhardt (2006) and $C = 2.10$, obtained by adopting the estimate of the tidal radius from Trager et al., since it is not provided by Noyola & Gebhardt. Dashed line: $r_c = 0.09'$ and $C = 2.05$, from McLaughlin & van der Marel (2005).

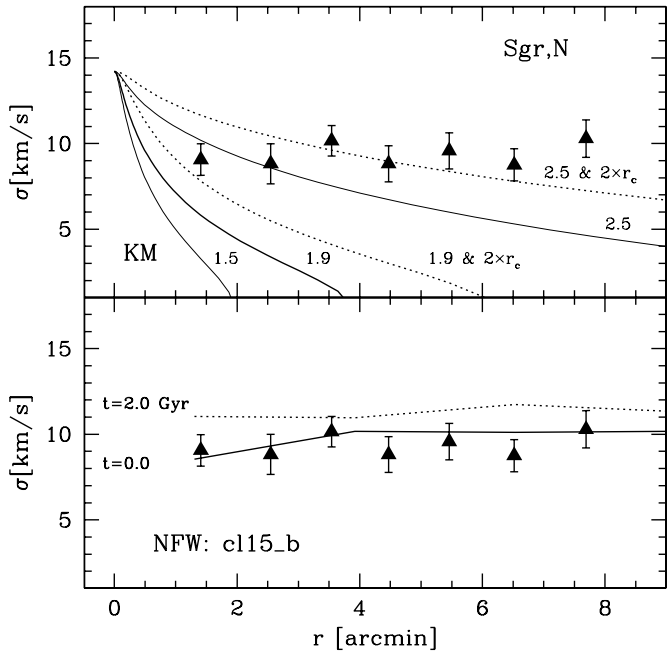

Figure 17. Comparison of the observed velocity dispersion profile of Sgr,N with theoretical models. Upper panel: comparison with King models of $r_c = 0.05'$ (best-fit value) and various C (thin continuous lines labeled with their C value), normalized at the central velocity dispersion of M54 ($\sigma_0 = 14.2$ km s^{-1}). The $C \sim 1.9$ case corresponds to the model that best-fits the observed SB profile and is plotted with a thicker line. The dotted curves show the effect on the profile of the assumption of r_c and r_t values much larger than the best-fit value (of factor $\times 2$). Lower panel: the observed velocity dispersion profile is compared with the profile of the Navarro et al. (1996, hereafter NFW) model adopted in the N-body simulation cl15_b (see Table 10). The profiles at the beginning (continuous line) and at the end (dotted line) of the simulation are shown.

some tidal harassment from the host galaxy (Sgr). In this case, some stars in the last bins would have been stripped from the outskirts of the cluster and heated up to the same dispersion of the surrounding field (see Muñoz et al. 2008, and references therein). In the lower left panel of Figure 14 the $\pm 3\sigma$ dispersion profiles of the best-fitting King model for M54 (Trager et al. 1995) are superposed on the M54 sample in the R versus V_r plane: the good match between the shape of the bulk of the observed distribution and the model profile out to the tidal radius strongly suggests that most of the velocity outliers at large radii are likely not gravitationally bound to the cluster, independent of their origin (unrelated metal-poor Sgr stars or former M54 members that have been tidally stripped).

While we consider the "contamination" hypothesis as more likely, the "tidal" hypothesis is a very fascinating possibility and it cannot be dismissed with the data we have presently in hand (see also Section 4.3).

Turning back to the inner regions of the cluster, the main conclusion we can draw here is that the observed velocity dispersion profile is consistent with the expected kinematics of the King models that best fit the light distribution of the cluster. Hence, M54 has the kinematics of an ordinary self-gravitating globular cluster, at least in its innermost ~25 pc, enclosing more than 90% of the cluster light/mass.

4.2.1. The Case of Sgr,N

In Figure 17 the observed velocity dispersion profile of Sgr,N is compared with various theoretical models. In the upper panel we compare King's models with $r_c = 0.05'$ and various values of the concentration parameter C (the best-fit model for the SB profile corresponds to $C = 1.9$). All the theoretical profiles have been normalized at the central velocity dispersion of M54: this is a quite arbitrary choice, the family of profiles can be shifted up and down according to the preference of the reader. It is clear that, independent of the adopted normalization, none of the plotted profiles provides a satisfactory match to the observations. The dotted profiles, reported here for comparison, show the effects of factor $\times 2$ changes in the adopted values of r_c and r_t. Even if such large values were compatible with the observations presented in Section 2 (and they are not), the corresponding profiles remain unable to reproduce the observed dispersions.

One could be tempted to suggest that any King model with a sufficiently large scale to fit the whole surface profile of the Sgr galaxy (as the $C = 0.90$, $r_c = 224'$ model by Majewski et al. 2003) would have a nearly flat dispersion profile on the relatively small radial range studied here ($r \leqslant 9'$), thus providing a reasonable fit to the observed profile. This is true, but these models would completely fail in reproducing the observed SB profile in the same range *by more than* 10 mag arcsec^{-2} (see Figure 2), since they lack any nuclear overdensity at their center.

Hence, contrary to the case of M54, King models that fit the SB profile of Sgr,N appear unable to reproduce its kinematics: this further supports the conclusion that M54 and Sgr,N are systems of very different nature.[18] In particular, as already noted, mass-follows-light models are incompatible with the observed velocity dispersion profile of Sgr,N (Gilmore et al. 2007).

In the lower panel of Figure 17 the observed profile is compared to those obtained from the N-body realization of a Navarro et al. (1996, hereafter NFW) model of the suite that is described in Section 5 (model NFW3, Table 10). The continuous line is the inner velocity dispersion profile of the NFW3 model

[18] We stress here that we are not attaching any particular physical meaning to King models while fitting Sgr,N profiles. This is just another way to put in evidence the differences between Sgr,N and M54 and a convenient reference model to parametrize the observed SB profile (Muñoz et al. 2008).

Table 10
N-Body Simulations: Fundamental Parameters and Results

Name	Halo	$M_{\rm halo}$ ($M_\odot$)	$N_{\rm halo}$	$M_{\rm clus}$ ($M_\odot$)	$N_{\rm clus}$	X_0 (kpc)	$V_{Y,0}$ (km s^{-1})	t_d (Gyr)	$t_{\rm tot}$ (Gyr)	ϵ_1	ϵ_5
bh2_a	NFW1	2.4×10^8	10^5	2.0×10^6	1	2.0	4.0	0.37	0.84	0.86	0.67
bh2_b	NFW1	2.4×10^8	10^5	2.0×10^6	1	2.0	8.0	0.74	1.28	0.73	0.52
bh2_c	NFW1	2.4×10^8	10^5	2.0×10^6	1	2.0	12.0	1.28	1.58	0.56	0.45
bh2_d	NFW1	2.4×10^8	10^5	2.0×10^6	1	4.0	4.0	1.22	1.28	0.87	0.65
bh2_e	NFW1	2.4×10^8	10^5	2.0×10^6	1	4.0	8.0	2.90	3.00	0.68	0.65
bh1_a	NFW1	2.4×10^8	10^5	1.0×10^6	1	2.0	4.0	0.67	0.74	0.83	0.72
bh1_b	NFW1	2.4×10^8	10^5	1.0×10^6	1	2.0	8.0	1.19	1.34	0.72	0.58
bh1_N	NFW2	6.1×10^7	10^5	1.0×10^6	1	2.0	4.0	2.25	2.50	0.36	0.13
cl1.2_N	NFW2	6.1×10^7	10^5	1.2×10^6	10^4	2.0	4.0	...	2.50	...	...
bh15_a	NFW3	4.2×10^8	10^5	1.5×10^6	1	2.0	4.0	0.80	1.00	0.76	0.71
bh15_b	NFW3	4.2×10^8	10^5	1.5×10^6	1	2.0	8.0	1.25	1.70	0.61	0.44
bh15_c	NFW3	4.2×10^8	10^5	1.5×10^6	1	2.0	12.0	2.05	3.00	0.40	0.36
bh15_d	NFW3	4.2×10^8	10^5	1.5×10^6	1	3.0	8.0	2.10	2.42	0.60	0.52
cl15_b	NFW3	4.2×10^8	10^5	1.5×10^6	10^4	2.0	8.0	...	2.00	...	...
bh10_b	NFW3	4.2×10^8	10^5	1.0×10^6	1	2.0	8.0	1.60	2.05	0.61	0.49
bh15_p	NFW3	4.2×10^8	10^5	1.5×10^6	1	5.0	12.0	–[a]	6.00	0.25	0.15
bh02_a	NFW3	4.2×10^8	10^5	2.0×10^4	1	2.0	4.0	–[b]	6.00	0.75	0.75

Notes. NFW1: $V_c = 30$ km s^{-1}; NFW2: $V_c = 15$ km s^{-1}. NFW1, NFW2: $a = 0.1$ and $b = 2.5$. NFW3: $V_c = 17$ km s^{-1}; $a = 0.5$ and $b = 15.0$. t_d: time at which the orbit is decayed to a distance from the center $r \leqslant 30$ pc. $t_{\rm tot}$: total time of the simulation. cl1.2_N: t_d cannot be defined as in the above cases since the cluster is no more self-bound at $t \gtrsim 0.8$ Gyr; at $t \sim 1.0$ the remnant is approximately at the center of the host halo. The case of cl15_b is analogous.

[a] At the end of the simulation the BH has reached a distance of ∼2 kpc from the center of the halo.

[b] The orbit of the BH remain stable over the whole duration of the simulations.

at the beginning of the simulation; the dotted line is the profile at the end of the simulation, i.e. after the complete orbital decay of a model of M54 that is launched in orbit within the NFW3 halo. It is interesting to note that the theoretical profiles are fairly flat in the considered radial range, in good agreement with the data. It may be conceived that the (baryonic) nucleus of Sgr lies within the inner cusp of the NFW halo of dark matter that is presumed to embed the Sgr galaxy (Ibata & Lewis 1998; Majewski et al. 2003, and references therein). The potential in this inner region would be dominated by the DM cusp that will impose the flat dispersion curve to the observed Sgr,N stars. It does not seem necessary to assume a strict correlation between the typical size and/or density profile of the DM cusp/core and those of the embedded stellar nucleus: the DM overdensity would have simply provided the "local" minimum of the overall potential well to "attract" the largest density of the infalling gas that formed Sgr,N. It may be interesting to note that the NFW3 model, whose velocity dispersion profile is shown in the lower panel of Figure 17, encloses a mass of $3.2 \times 10^6\ M_\odot$ within the range of projected radii covered by our data ($r_p \simeq 70$ pc), and that the region in which its projected density profile is well fitted by a power-law, i.e. the inner cusp, has a size of $r_p \lesssim 100$ pc, similar to Sgr,N.

Unfortunately, we have no conclusive observational evidence in support of the above scenario. Note also that a DM halo with a core much larger than the nuclear scale would also display a flat dispersion curve in this region (as discussed above for the case of the $C = 0.90$, $r_c = 224'$ King model); it is just the small-scale inner cusp as a possible seed for the formation of a barionic nucleus that can make the NFW option slightly more attractive.

A flat velocity dispersion profile may arise as a consequence of strong tidal disturbance, in mass-follow-light models of dwarf galaxies (Muñoz et al. 2008). While Sgr is clearly in course of tidal disruption, here we are dealing with the kinematics of the innermost ≃70 pc of the galaxy, that should (reasonably) be considered as untouched by the Galactic tides, since the tidal radius of Sgr is as large as a few thousands of parsecs (the formal King's major axis limiting radius is $r_t \gtrsim 10$ kpc, according to Majewski et al. 2003).

Finally, it may appear as a curious coincidence that M54 and Sgr,N have similar spatial scales, if they have independent origin. In this sense we can only note that the distributions of sizes and luminosities of globular clusters and stellar galactic nuclei largely overlap, so the observed similarity may not be particularly odd (see Federici et al. 2007; Böker 2008). Moreover, it should be noted that the core and half-light radii of M54 are ∼2 times larger than those of Sgr,N, clearly a non-negligible difference. Finally, while the best fitting King models have essentially the same C parameter, the two observed profiles appear to have significantly different slopes at large radii, where the profile of Sgr,N departs from the King model.

4.3. Rotation

We searched for signals of rotation in the two samples, also taking into account the correction for perspective rotation, according to van de Ven et al. (2006) and taking the proper motion of Sgr/M54 from Dinescu et al. (2005); in the present case the absolute value of the maximum correction is $\leqslant$1.0 km s^{-1}. Given a rotation of the coordinate axes by an angle θ

$$\eta = X\cos(\theta) - Y\sin(\theta)$$
$$\chi = X\sin(\theta) + Y\cos(\theta)$$

we tried all the possible values of θ in steps of 1°. For each adopted θ we computed the median velocity of stars with negative and positive η. The difference between the two median velocities is a robust measure of the amplitude of any systemic motion around an axis tilted by θ degrees from the χ axis, i.e. of the rotation of stars about this axis.

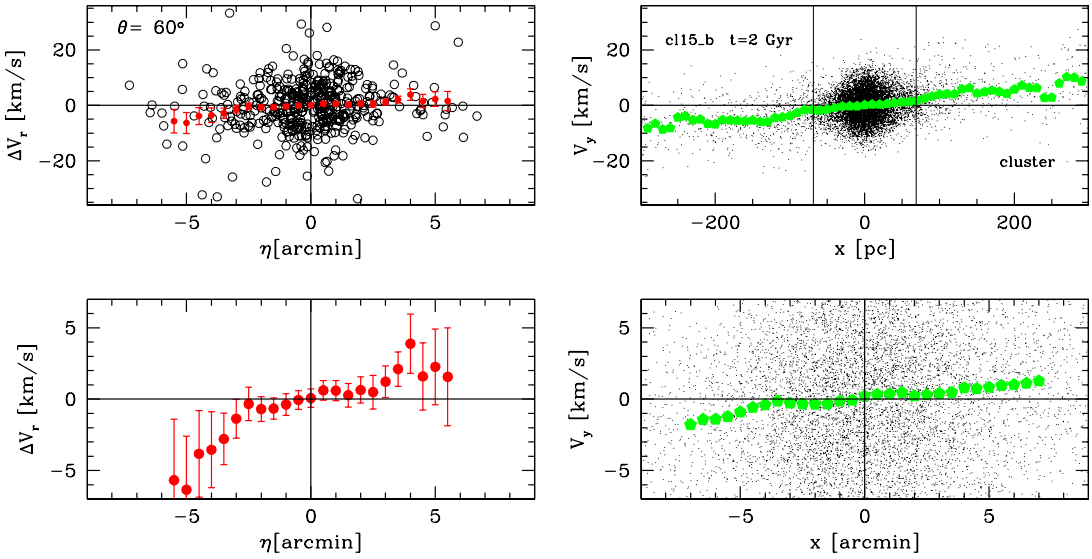

Figure 18. Left panels: Rotation curve of M54 assuming a rotation axis tilted by $\theta = 60^\circ$ east of north. ΔV_r is the difference between the observed radial velocity and the global mean systemic velocity of Sgr,N ($\langle V_r \rangle = \mathrm{km\ s^{-1}}$). Upper panel: individual stars. Lower panel: running mean with bin width of 2′ and step of 0.′5. Right panels: rotation in the remnant of the model of M54 at the end of the simulation cl15_b. The coordinate system is chosen such that x, z projects on the plane of the sky while y is along the LOS and the orbit of the cluster is in the x, y plane. Upper panel: LOS velocity as a function of x for the innermost 300 pc. The vertical thin lines enclose a region of the same dimension as the one studied here; the large dots are the running mean of the velocity computed with the same bin width and step as in the real case. Note the tidal tails emerging from the main body of the remnant at $x \sim \pm 50$ pc. Lower panel: zoomed view of the inner region of the plot. In this case x has been converted in arcmin by placing the remnant at the same distance as the real cluster. The diagram has the same scale as the lower left panel for an easy comparison.

(A color version of this figure is available in the online journal.)

In some cases, ordered patterns of V_r as a function of η emerged (in particular for the M54 sample), but their amplitude was quite weak, typically lower than 2.0 km s^{-1}. While we can clearly exclude the presence of rotation signals stronger than this, we cannot exclude that such weak patterns are in fact real. In Figure 18 we show the best case for the M54 sample compared with the end product of one of the N-body simulations that are described in Section 5. We refrain from attaching any significance to such a weak pattern, in particular as it has an amplitude similar to the typical uncertainty of the individual velocity measures and is much weaker than the typical velocity dispersion of the sample. We just want to draw the attention of the reader to the fact that the orbital decay of a massive cluster within the parent dwarf galaxy seems to naturally produce these kinds of weak velocity gradients in the inner part of the sinking cluster at the end of the decay process (see Muñoz et al. 2008, for a deeper discussion of the effects of tidal disruption). However, it is quite clear that the detection at $r \gtrsim 10'$ of stars having metallicity compatible with M54, possibly lower velocity dispersion than the surrounding metal-rich Sgr population, and, above all, having significant differences in mean systemic velocity compatible with a tidally induced rotation like that shown in the upper right panel of Figure 18, would be the final "smoking-gun" of the orbital decay of M54 to its current position. On the other hand, the failure to find such a component would not be sufficient to rule out the hypothesis as, for instance, the density of stars in the tidal tails is expected to be *very* low and the "rotation" signal may be greatly weakened by unfavorable orientations of the orbital plane with respect to the LOS (Muñoz et al. 2008).

5. THE KINEMATICS OF M54 AND Sgr,N: N-BODY SIMULATIONS

M05a used simple analytical formulae to verify the plausibility of the hypothesis that the "exact" coincidence between the positions of M54 and Sgr,N is due to the cluster progressively spiraling into the center of density of the Sgr galaxy due to dynamical friction. They found that the observed status of the globular cluster system of Sgr is in full agreement with this hypothesis. The orbit of the massive M54 cluster is expected to decay completely within one Hubble time if it is born within three core radii (∼5 kpc) from the center of Sgr, while the other, much less massive Sgr clusters (Ter 7, Ter 8, Arp 2) would be essentially unaffected by dynamical friction if they were born outside one core radius. While promising, this first result demands further investigation. One very interesting question, for instance, is: does the actual orbital decay of M54 under realistic conditions lead to such a nearly perfect coincidence between M54 and Sgr,N as observed? To answer questions like this we performed the suite of N-body simulations that is described in detail below. While examining the results of our N-body experiments it should be carefully considered that:

1. The main purpose of our simulations is to study the effect of dynamical friction in the specific case of M54 orbiting within the Sgr galaxy, with particular focus on the final status of the system. Detailed and more general theoretical analyses of the effects of dynamical friction on globular clusters within a dwarf galaxy can be found in Oh et al. (2000), Read et al. (2006), Fujii et al. (2006), Miocchi et al. (2006), and Sánchez-Salchedo et al. (2006), and references therein.
2. We do not intend our simulations to be exhaustive of all the possible cases. This would be prohibitive since, for example, we do not even know the total mass of the bound part of the Sgr galaxy (see Majewski et al. 2003, and references therein). Our aim is to verify if a broadly realistic case can produce the final outcome we actually observe, i.e. a cluster that has nearly exactly the same position and *velocity* as the nucleus of its host galaxy.

3. Here we study the case of a massive cluster orbiting within a model of the Sgr galaxy which evolves in isolation. We verified that this assumption does not seriously affect our main results. We replicated some of our experiments launching the Sgr model into a realistic (but static) Galactic potential (model 2d of Dehnen & Binney 1998): we found that if M54 was not lost into the tidal tails of the disrupting Sgr galaxy (as it happened for some Sgr clusters, see Bellazzini et al. 2003a), it plunged to the center of Sgr approximately on the same timescales as the isolated models.
4. A detailed comparison with the existing literature on dynamical friction would be clearly beyond the scope of the present paper (see, for instance, Colpi et al. 1999, and references therein). In the present context, suffice to say that our results are in reasonably good agreement with the analytic estimates by M05a as well as with the results by Oh et al. (2000); Sánchez-Salchedo et al. (2006); Read et al. (2006, and references therein).

5.1. General Features of the N-body Experiments

The simulations were performed with `falcON`, a fast and momentum-conserving tree-code (Dehnen 2000, 2002), within the NEMO environment (Teuben 1995). Gravity was softened with the kernel "P_2" (Dehnen 2000), with a softening length of 3 pc (except for two special cases, bh_15p and bh_02a, discussed in Section 5.2). The minimum time-step was 1.9×10^{-6} Gyr, and the tolerance parameter $\theta = 0.6$.

To model the Sgr galaxy we adopted a truncated NFW model of the form

$$\rho(r) \propto \frac{\mathrm{sech}(r/b)}{r(r+a)^2}\,.$$

For the model NFW1, the parameters $a = 0.1$ kpc, $b = 2.5$ kpc, were selected, which together with a maximum circular speed of $V_c = 30$ km s^{-1}, gives a total mass of $M_{\rm TOT} = 2.4 \times 10^8\,M_\odot$. This rather massive model was chosen to approximate to the sort of dense system suggested by Ibata & Lewis (1998) that would not be rapidly destroyed by Galactic tides. A second, lower-mass system (NFW2) with $a = 0.1$ kpc, $b = 2.5$ kpc, and $V_c = 15$ km s^{-1} ($M_{\rm TOT} = 6.1 \times 10^7\,M_\odot$) was also simulated. The motivation for this second model was that the central velocity dispersion in this case should be similar to the observed dispersion of Sgr (while keeping a and b identical to the first model). The NFW3 with $a = 0.5$ kpc, $b = 15.0$ kpc, and $V_c = 17$ km s^{-1} was chosen to have both a size and a central velocity dispersion similar to the present-day main body of Sgr, irrespective of its robustness to Galactic tides.

In all cases the NFW halos were modeled with 10^5 particles. M54 was modeled as a single massive particle of 1, 1.5, or 2 million solar masses, as if it were a black hole (*bh* simulations, as opposed to cl simulations, see Table 10 and Section 5.2). The particle is launched within the NFW halo from $(x, y, z) = (2, 0, 0)$ kpc or $(4, 0, 0)$ kpc[19] (note that the core radius of Sgr is $r_c \simeq 1.7$ kpc Majewski et al. 2003), with velocities in the y direction in the range 4.0 km s^{-1} $\leqslant V_y \leqslant$ 12.0 km s^{-1}, while $V_x = V_z = 0.0$ km s^{-1}, hence the orbits of the M54 models lie in the x, y plane. As a mere convention to simplify the discussion, we consider the y direction coincident with the LOS between us and the center of Sgr, and the x and z directions as projected on the plane of the sky. When needed we will select particles according to their projected radius $r_p = \sqrt{x^2 + z^2}$.

The initial conditions of the various simulations are reported in Table 10. The simulations were usually stopped when it was clear that the orbit of the M54 particle had reached a stable configuration at the center of the host halo($t_{\rm tot}$). The *decay time* (t_d) is defined as the epoch at which the 3D apocentric distance of the M54 particle become $r_{\rm apo} \leqslant 30$ pc. Note that around this limit the adopted time step becomes too small with respect to the orbital period of the infalling massive particle, hence the evolution of the orbit cannot be followed further. To provide a quantitative idea of the evolution of the eccentricity of the orbit ($\epsilon = (r_{\rm apo} - r_{\rm peri})/(r_{\rm apo} + r_{\rm peri})$) we report the eccentricity at the first (ϵ_1) and fifth (ϵ_5) pericentric passages. The evolution of the orbital radius and of the average velocity of the M54 models is shown in Figure 19.

5.2. The Evolution of the Orbit of M54 Models

From the inspection of Table 10 and Figure 19 we can draw the following conclusions:

1. In spite of the wide range of initial conditions that has been explored, the orbit of all the M54 models decayed completely in less than 3 Gyr (5–15 orbits). At the end of our simulations M54 is always virtually *at rest* (mean velocity $\lesssim$1–2 km s^{-1}) at the very center of the host halo (within a few softening lengths). Hence the hypothesis that M54 has reached its presently observed status by dynamical-friction-driven orbital decay appears completely realistic and viable (within the limitations imposed by the resolution of our N-body experiments).
2. Two special simulations (bh15_p and bh02_a) have been performed at a lower resolution (softening length of 10 pc) as the BH was not expected to reach the densest regions of the host halo (NFW3). bh15_p explores the case of a M54-like point mass decaying from somehow extreme initial conditions (large distance $x_0 = 5.0$ kpc and high velocity $V_{y,0} = 12.0$ km s^{-1}). In six Gyr the orbit of the BH is sufficiently decayed to bring it within 2 kpc from the center of the halo. The other simulations indicate that from this point it will require less than 3 Gyr to reach the very center of the halo. From the bh15_p simulation we can deduce that for starting distances larger than 5.0 Kpc the times required for a complete decay begin to be comparable to the Hubble time, in good agreement with the results by M05a, and also that it is quite possible that M54 has reached the very center of Sgr only in recent times, if it was born sufficiently far away from the center. The analytical computations by M05a also indicated that clusters with a mass similar to the other GC residing in the main body of Sgr (Ter 7, Arp 2, Ter 8, $M \leqslant 2. \times 10^4\,M_\odot$) would have infinitely long decay times (i.e. stable orbits) if they born at $r \gtrsim 1$ kpc from the center of Sgr. As the closest of these clusters lie at ∼2.9 kpc from the center of Sgr, M05a concluded that all of them are on stable orbits. Simulation bh02_a is intended to verify this conclusion by letting a BH as massive as the most massive Sgr cluster (except M54, i.e. Arp 2, $M \lesssim 2. \times 10^4\,M_\odot$, adopting the same $(M/L)_V$ of M54, which seems appropriate given the age and metallicity of the cluster) evolve from a starting point

[19] In the coordinate system in which $(x, y, z) = (0, 0, 0)$ kpc corresponds to the center of density of the model halo and a point having $(V_x, V_y, V_z) = (0, 0, 0)$ km s^{-1} is at rest with respect to the center of the system. The adopted range of initial distances from the center of the parent galaxy is typical of the other clusters residing in the main body of Sgr (Ter 7, Arp 2, Ter 8) which are located between ∼3 kpc and ∼5 kpc from the center of Sgr and should have orbits that are stable against dynamical friction (see M05a and below).

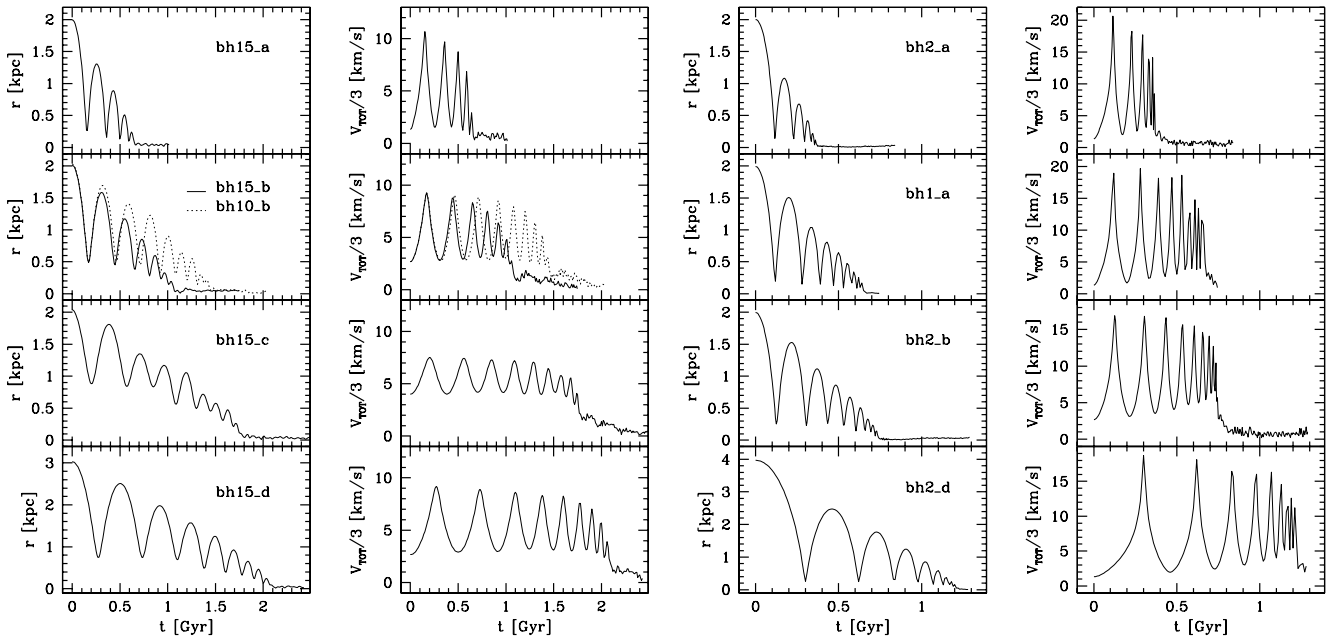

Figure 19. Orbital evolution of the single massive particle representing M54 in the N-body experiments described in Table 10. Left panels: distance from the center of the host NFW halo as a function of time. Right panels: mean one-component velocity of the massive particle $\frac{V_T}{3}$ as a function of time, where $V_T = (V_x^2 + V_y^2 + V_z^2)^{\frac{1}{2}}$.

$x_0 = 2.0$ kpc and a low initial velocity ($V_{y,0} = 4.0$ km s^{-1}). After 6 Gyr no sign of decaying is noticed and the orbit is absolutely stable, in excellent agreement with the results of M05a.

3. The effect of dynamical friction is to progressively decrease the radius, the period, and the eccentricity of the orbit. The mean velocity, on the other hand, appears to drop suddenly in the last phases of the decay, possibly when the point-mass particle reaches the dense central cusp of the host NFW halo. This may suggest that the presence of a central cusp may be a crucial ingredient to lead to the observed phase-space coincidence between M54 and Sgr,N, in particular if the recent results by Sánchez-Salchedo et al. (2006) and Read et al. (2006) are considered. This suggestion is worth being followed up with specific high-resolution simulations adopting different kinds of host galaxy halo models (such as King models, for instance). Recent studies indicate that dynamical friction is probably much less efficient in cored than in cusped structures (see Sánchez-Salchedo et al. 2006; Read et al. 2006; Goerdt et al. 2006).

To check the impact of our adoption of a point-mass model of M54, we repeated the simulation bh1_N and bh15_b adopting a 10^4 particle King model resembling the real cluster as much as possible ($W_0 = 8.0$, $r_t = 60$ pc; simulations cl 1.2_N and cl 15_b of Table 10); in the case of cl1.2_N the mass was adjusted to $M = 1.2 \times 10^6\ M_\odot$ to have a central LOS velocity dispersion of $\sigma_0 \simeq 15$ km s^{-1}. All the final results are fully consistent with those obtained in simulations with a point-mass model for M54, hence for the purposes of the present study, we do not further distinguish between these two classes of models. To illustrate the typical behavior of these live M54 models in Figure 20 we show a series of snapshots of the evolution of the cluster model of simulation cl15_b. It is interesting to note that in this simulation (as well as in the cl1.2_N one) the cluster suffers strong tidal disruption from the host halo and the final relic sitting nearly at rest at the center of the halo is probably unbound, at odds with the real case. The very fact that the actual cluster is still bound may provide useful constraints on the mass distribution within the Sgr galaxy, which can probably be explored with a systematic suite of N-body simulations.

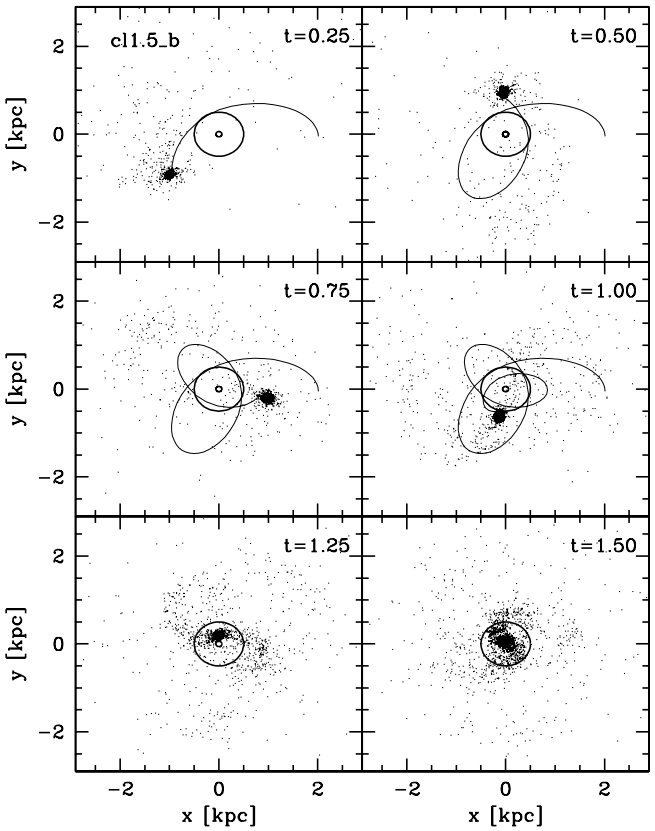

Figure 20. Evolution of the M54 cluster model within the NFW model of the Sgr galaxy, for the simulation cl1.2_N (see Table 10). In each snapshot of the x, y distribution we plot only the points of the M54 model, for clarity. Concentric circles of radius 60 pc and 500 pc are plotted in each panel, for reference. In the top four panels we also plotted the orbit of the bh1_N model to show the approximate path of the center of mass of the cluster model.

6. SUMMARY AND DISCUSSION

We present the results of a large radial velocity survey of stars in the nucleus of the Sgr galaxy and in the globular cluster M54, which lies at the center of the nucleus itself. From high S/N Keck-DEIMOS and VLT-FLAMES spectra, we obtained accurate radial velocities ($\epsilon_{V_r} \simeq 2$ km s^{-1}) and metallicities from the Ca triplet for 1152 candidate RGB/RC stars of M54/Sgr,N. Selecting by the position in the CMD, by radial velocity and by metallicity, we obtained two reliable and clean samples of 321 Sgr,N members and 425 M54 stars and we used these samples, further cleaned of 3σ velocity outliers, to study the kinematics of the two systems.

In support of this analysis we used archival *HST*/ACS images to refine the estimates by M05a of the structural parameters of Sgr,N.

We also performed a suite of N-body simulations of the orbital decay (driven by dynamical friction) of a massive cluster into a host dwarf spheroidal galaxy, mimicking the M54–Sgr system. We focused our attention on the possibility to realize a phase-space match between the infalling cluster and the density cusp of the host NFW halo as close as that observed with M54 and Sgr,N.

The main results of our analyses can be summarized as follows:

1. We have obtained new, much more reliable estimates of the total luminosity and of the typical size of Sgr,N, confirming that it is significantly less luminous than M54 and that it has a different luminosity distribution with respect to the cluster.
2. The systemic radial velocities of M54 and Sgr,N are identical within $\sim\pm1$ km s^{-1}. Coupling this result with those by M05a, it appears that the two systems coincide in phase-space to within the observational errors, at least for what concerns position in space and radial velocity.
3. The velocity dispersion profile of M54 is in good agreement with the theoretical profile of the King model that best fits its surface brightness, at least over a range of 30 core radii ($r \leqslant 3.5'$), but possibly also beyond this radius (see Section 4.2). In particular, the velocity dispersion drops from $\sigma = 14.2$ km s^{-1} at $r = 0$ to $\sigma \simeq 5.3$ km s^{-1} at $r \sim 3.5'$. The observed velocity profile strongly suggests that M54 behaves as an ordinary, self-bound globular cluster, at least in its innermost and densest region. In our view, this indicates that even if at the present epoch the motion of its stars is driven by the potential produced by the overall mass distribution within Sgr,N (see below), its velocity profile keeps memory of its original nature as an ordinary massive globular cluster orbiting within the Sgr galaxy. A turn-over of the profile to $\sigma = 8.8$ km s^{-1} around the tidal radius of the cluster may suggest that some degree of tidal disruption is occurring in the outskirts of the cluster; however, the alternative hypothesis that the sample is contaminated by metal-poor Sgr stars at large radius is also viable and seems more likely at the present stage (Section 4.2).
4. The velocity dispersion profile of Sgr,N is consistent with being flat at $\sigma \simeq 10$ km s^{-1} over the whole considered radial range ($r \leqslant 9'$). The profile is hardly compatible with any realistic King model roughly reproducing the observed SB profile of Sgr,N. More generally, the fact that the velocity profile is flat in a radial range in which the surface density declines by a factor of >1000 is strongly uncompatible with any mass-follows-light model (Gilmore et al. 2007). Conversely, a realistic NFW model reasonably reproduces the observed velocity profile and, in principle, does not conflict with the presence of an overdensity of baryons at its center, like Sgr,N. However, it has to be recalled that the NFW model does not make any definite prediction on the SB profile of the embedded stellar nucleus and the compatibility of the observed SB profile of Sgr,N with the NFW model that that fits the velocity profile is not established.
5. M54 and Sgr,N have definitely different kinematical properties. In particular, the velocity dispersion profiles are very different: in the radial range $1.5' < r < 6.5'$ the statistical significance of the difference in the velocity distribution is very large.
6. We have provided observational evidence that the velocity dispersion profile of Sgr remains flat from $r \simeq 1'$ to $r \simeq 100'$ and that there is no apparent transition in the velocity profile corresponding to the onset of the stellar nucleus, at $r \lesssim 10'$. This fact as well as those listed above strongly suggest that Sgr,N and M54 had independent origins, as we would expect that, if the cluster provided the mass seed to collect the Sgr gas that later formed the metal-rich nucleus, Sgr,N stars would have shown a declining velocity dispersion profile, compatible with a mass-follows-light distribution.
7. Our N-body simulations that follow the orbits of massive clusters ($1–2 \times 10^6\ M_\odot$, representing M54) within different NFW halos (representing the Sgr galaxy) show that for a large range of initial distances and relative velocities, the orbit of the cluster decays completely by dynamical friction within 3 Gyr, at most. Moreover, at the end of the simulations, the cluster is perfectly concentric with the cusp of the host halo (within the resolution of the simulation) and the difference in average velocity is always less than ~2 km s^{-1}. Hence, the observed phase-space coincidence between M54 and Sgr,N can be naturally explained by the "dynamical friction hypothesis" (M05a).
8. According to FC06, the mass of central massive objects, independently if they are black holes or stellar nuclei, is $\simeq\frac{3}{1000}$ of the mass of the host galaxy $\left(\frac{M_{\rm CMO}}{M_{\rm gal}} = 0.003\right)$. Using our estimates for the total mass of Sgr,N and M54 we obtain the following estimates for the total mass of the Sgr galaxy, depending on whether we assume is the M54, Sgr,N or the sum of the two (as we would do if we observed the system at the distance of the Virgo cluster) is the central massive object (CMO), $M_{\rm Sgr} = 1.0 \times 10^9\ M_\odot$, $M_{\rm Sgr} = 2.1 \times 10^9\ M_\odot$, and $M_{\rm Sgr} = 3.0 \times 10^9\ M_\odot$, respectively. These values are in very good agreement with the independent estimates by Majewski et al. (2003) that ranges from $M_{\rm Sgr} = 5.8 \times 10^8\ M_\odot$ to $M_{\rm Sgr} = 6.9 \times 10^9\ M_\odot$. Hence both Sgr,N and M54 singularly or taken together have a mass compatible with being the CMO of the Sgr galaxy.
9. Both Sgr,N and M54, as well as the combination of the two, when placed in the M_V versus $\log r_h$ diagram lie in a region that is populated by globular clusters *and* galactic stellar nuclei. They are also compatible with the color–magnitude relation of nuclei shown by FC06 and with the M_V versus σ relation satisfied by globular clusters, nuclei, and UCDs (see Geha et al. 2002; Evstigneeva et al. 2007), as shown in Figure 21. Hence the structure and dynamics of Sgr,N,

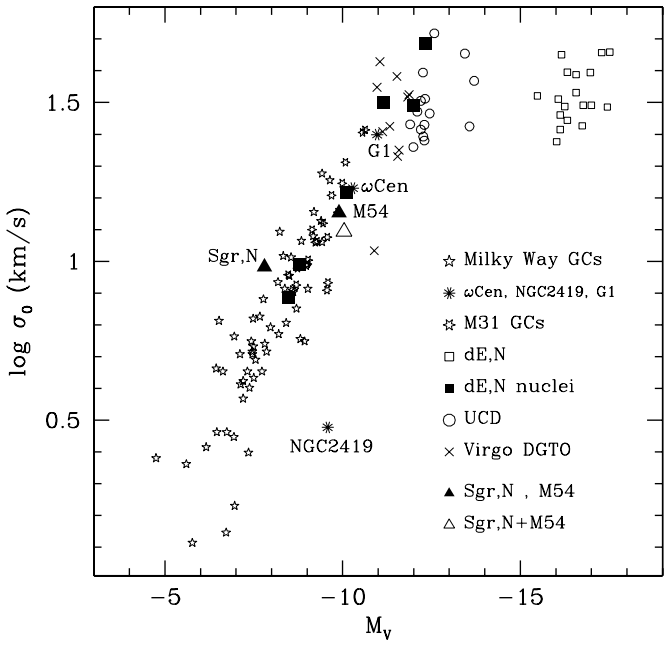

Figure 21. Sgr,N and M54 (filled triangles) in the M_V vs. σ plane (see Evstigneeva et al. 2007). Both systems lie on the locus common to globular clusters, dE nuclei, Dwarf-Globular Transition Objects (DGTO Hasegan et al. 2005), and, possibly, UCDs. The same is true for their combination (Sgr,N+M54, open triangle), i.e., for a system having luminosity equal to the sum of the luminosities of M54 and Sgr,N and having σ as estimated from an integrated spectrum obtained with a $1''$ slit from the distance of the Virgo cluster of galaxies ($\sigma \simeq 12.4$ km s^{-1}). Data for galactic globulars are from Mackey & van den Bergh (2005, M_V) and Pryor & Meylan (1993, σ); for M31 globulars we took integrated magnitudes from the Revised Bologna Catalog (Galleti et al. 2004) and σ from Djorgovski et al. (1997); data for dE and dE,N are from Geha et al. (2002, 2003); UCDs data are from Drinkwater et al. (2003) and Evstigneeva et al. (2007); data for DGTO are from Hasegan et al. (2005). Some remarkable bright clusters have been labeled, for reference (see Federici et al. 2007).

M54 and their combinations are fully compatible with other galactic nuclei.

10. A detailed study of the mass profile of Sgr,N and M54 using the Schwarzschild method (see Rix et al. 1997; van de Ven et al. 2006, and references therein) is currently ongoing and the results will be presented elsewhere (R. A. Ibata et al. 2008, in preparation).

These findings lend very strong support to the scenario proposed by M05a to explain the M54/Sgr,N system: the nucleus of the galaxy formed *in situ*, at the bottom of the potential well of the Sagittarius galaxy; the globular cluster M54 was independently driven to the same site by dynamical friction. As a complement of the above conclusions, it must be recalled that the stellar population that dominates Sgr,N formed several Gyrs later than M54 (see Montegriffo et al. 1998; Sarajedini & Layden 1997; Layden & Sarajedini 2000; Bellazzini et al. 2006a; Siegel et al. 2007, and references therein). In the present context this does not appear particularly relevant, but it should be kept in mind that M54 could have reached the very center of Sgr *after* Sgr,N formed its stars (within the last ∼5–9 Gyr Bellazzini et al. 2006a), or even *before* this, depending on the birthplace of the cluster within the Sgr galaxy. In any case it is very likely that both the cluster and the processed Sgr gas were *independently* driven, by different mechanisms, to the bottom of the potential well of the Sgr galaxy, i.e. to the center of its dark matter halo. A conclusive proof that M54 was driven to its present position by dynamical friction could be provided by the successful detection of genuine extra-tidal stars at large distances from the cluster center as envisaged in Section 4.3, while, as said, their non-detection will not disprove the above scenario.

As a possible alternative to this view (or as an extreme version of it) it can be conceived that M54 formed at the bottom of the overall potential well of the Sgr galaxy since the beginning. In this framework M54 and Sgr,N are just the results of two subsequent episodes of star formation both occurring at the very center of Sgr, the second from enriched gas that was infalling on very different orbits with respect to the gas that formed M54, thus resulting in different final stellar kinematics. We regard this possibility as much less likely with respect to the "dynamical-friction" scenario depicted above. First, if M54 is considered as part of the (metal-poor) field population of Sgr, its presence would be at odds with the global metallicity gradient observed by Alard (2001), Bellazzini et al. (1999), Sarajedini & Layden (1997) and others in Sgr, as well as in all dwarf spheroidal galaxy studied to date (more metal rich and younger populations are preferentially found at the center of dSph's Harbeck et al. 2001). While dE nuclei have been indicated as a possible exceptions to this trend, the ingestion of large metal-poor globular clusters in pre-existing metal-rich nuclei seems one possible natural way to reconcile the generally observed metallicity gradients and the presence of nuclei that are bluer than their parent galaxy (Lotz et al. 2004). Second, as both M54 and Sgr,N would have *formed* from gas falling into the same potential well, the reason for the different kinematics remains to be explained, while it is a natural outcome if M54 formed elsewhere as a classical globular cluster.

6.1. The Process of Galaxy Nucleation

If we take as demonstrated the above concluding remarks, we can ask what we have learned about the process of galaxy nucleation from the case studied here. Concerning the two main mechanisms that have been put forward in the literature, i.e., (a) formation of the nucleus by infall of globular cluster(s) to the center of the galaxy, or (b) *in situ* formation by accumulation of gas at the center of the potential well and its subsequent conversion into a stellar overdensity (see Section 1 and Grant et al. 2005; Côté et al. 2006), the main conclusion that can be drawn from the case of Sgr is that both channels are viable and actually both have been at work "simultaneously" in Sgr.

The present analysis has shown that a stellar nucleus made of the typical material that dominates the baryonic mass budget of Sgr is present in this galaxy, independent of M54, as it displays the same flat velocity dispersion profile as the whole core of Sgr, much different than that of the cluster.

In a likely scenario, the enriched gas from previous generations of Sgr stars accumulated at the bottom of the overall potential well of the galaxy, until star formation transformed it into a stellar nucleus whose SB is $\gtrsim$100 times larger than in the surrounding Sgr core—a substructure within a larger galaxy. On the other hand, M54 is a (relatively) ordinary massive, old and metal-poor globular cluster. Independent of its birthplace within the early Sgr galaxy, its mass and the density of the surrounding medium of the host galaxy drove it to the bottom of the Sgr potential well by dynamical friction. During its trip to the densest central region of Sgr, the dense cluster managed to survive the tidal force of the host galaxy, hence it reached the present position as a (partially?) self-bound stellar system.

While the mass budget at the center of Sgr is probably dominated by the underlying DM halo, M54 dominates the

overall light distribution: an observer taking photometry and/or spectra of the unresolved nucleus of Sgr from a distant galaxy (say, a galaxy in the Virgo cluster) would find that the object looks like a bright and blue globular cluster; the integrated velocity dispersion would not show any peculiar feature revealing the composite nature of the observed nucleus (see Figure 21). It would probably be impossible to disentangle the two systems from the integrated light.[20]

Finally, the Sgr case seems to support the observed ubiquity of nuclei (see Section 1 and C06). The Sgr galaxy was able to form a sizable nucleus "twice" and with two different formation channels: if either of the two channels had not been viable for some reason, the galaxy would have ended up with a nucleus in any case. The fact that Sgr is the only case of galaxy with a clear nucleus among those classified as dwarf spheroidals in the Local Group may suggest that the progenitor of Sgr was in fact a brighter dE or disc galaxy that has been transformed into a dSph by the interaction with the Milky Way (Majewski et al. 2003; Mayer et al. 2007, M05b, and references therein)

6.2. Suggestions for Further Investigations

The results presented in this paper suggest several interesting lines of research that we did not follow up for practical reasons. However, we feel that it is worth briefly mentioning some of them here, as a possible starting point for future studies.

1. The results presented by Read et al. (2006), Goerdt et al. (2006), and Sánchez-Salchedo et al. (2006) suggest that the complete decay of a massive cluster to the very center of the host galaxy is much easier and faster if a central density cusp is present. It is even possible that a central cusp is actually *required* to bring a cluster down to the very bottom of the overall potential well. If this is the case, the position of M54 within Sgr,N would support the existence of a central cusp in actual DM halos, a point that has been questioned by several authors (see Sánchez-Salchedo et al. 2006, and references therein). The "complete infall" of a massive cluster may need a NFW cusp and, simultaneously, it may transform the cusp into a core by transferring orbital energy and momentum to the surrounding "medium", thus possibly providing a self-regulating mechanism that simultaneously prevents the further decay of other clusters (that, in general cases, would be quite difficult, given the expected decay times, see Hernandez & Gilmore 1998; Oh et al. 2000; Read et al. 2006; Sánchez-Salchedo et al. 2006; Goerdt et al. 2006, and references therein). In this context, it may also be worth recalling the work by Strigari et al. (2006), whose results militates against the presence of a large-size core in the Fornax dSph, and by Boylan-Kolchin & Ma (2004) on the resilience of cuspy halos in major mergers. These ideas seems worthy of detailed theoretical follow-up.
2. It has been suggested several times that bright and metal-poor globular clusters may be of cosmological origin (see Brodie & Strader 2006; Maschenko & Sills 2005, and references therein). If this is the case, they may be very intimately linked to the earliest phases of formation of galaxies and there may have been plenty of opportunities for most of them to become the nuclei of some dwarf galaxy. The tidal stress that they suffered during their infall to the center of their host galaxies may be at the origin of the larger half-light sizes that are observed in those that have been suggested as possible nuclear remnants of ancient dwarf galaxies (Freeman & Bland-Hawthorn 2002; Federici et al. 2007; Mackey & van den Bergh 2005). This kind of scenario may be explored with dedicated N-body simulations, possibly including gas and stars. It would be interesting also to consider in detail the results presented here in relation with the scenario for the origin of globular clusters recently discussed by Böker (2008).
3. All the analysis presented in this paper have been performed within the standard Newtonian gravitation theory and dynamics. It may also be worthwhile to consider the observational scenario that emerged from this study in the framework of Modified Newtonian Dynamics paradigms (MOND, see Milgrom 2008; Sanders & McGaugh 2002, and references therein), even if it may not necessarily be an ideal case. The transition between the ordinary Newtonian regime and MOND regime occurs around $r \simeq 4.5'$–$6.5'$ (a range covered by our data), depending on the actual stellar mass of M54+Sgr,N.
4. There is little doubt that the final fate of the Sgr galaxy will be its complete tidal disruption. Once the large-scale stellar body of Sgr will be completely dispersed into the Galactic halo, the final remnant of this (once) relatively large galaxy would be a faint nucleus embedding a bright globular cluster. An observer lacking any knowledge of the origin of this object would conclude that it is a very bright and peculiar globular cluster, dominated by a metal-poor population ([Fe/H] ~ -1.5, possibly with some spread) but also including a small fraction ($\sim$10%) of metal-rich stars (with average [Fe/H] ~ -0.4). Also the abundance patterns would appear different: for instance, the metal-poor (M54) stars would appear as moderately α-enhanced (Brown et al. 1999), while metal-rich stars (Sgr,N) would have solar or subsolar [α/Fe] ratios (M05b). The radial velocities would reveal that the metal-rich and metal-poor stars have *the same systemic velocity*, but *different velocity dispersion profiles* and slightly different density profiles, possibly with some rotation in the metal-poor component. However, the dominance of metal-poor (M54) stars would be so high that there would be no hint of the presence of a dark matter component. The half-light radius of the system would appear slightly larger with respect to ordinary globulars (Mackey & van den Bergh 2005; Federici et al. 2007). Most of these likely characteristics of the future remnant of Sgr seem to have a counterpart in the widely studied and mysterious stellar system ω Centauri (see Norris et al. 1997; van Leeuwen et al. 2002; Pancino et al. 2000, 2002, 2003; van de Ven et al. 2006, and references therein), which has been proposed as the possible remnant of a nucleated dwarf elliptical since the work of Freeman (1993). While there are also noticeable differences between the two cases, the analogy seems very intriguing and potentially powerful.[21] It is possible that at least some

[20] It would be interesting to check if there is some spectral feature that may reveal the composite nature of the "system," in the present case. We plan to do this in the future by combining properly scaled synthetic spectra representing the light output of M54 and Sgr,N.

[21] It is interesting to recall that ω Cen shares with Sgr some remarkable chemical peculiarities. In particular, stars of comparable metallicity in the two systems are strongly enhanced in s-process elements and the ratio of heavy s-process to light s-process elements [hs/ls] is very similar. Furthermore, ω Cen and Sgr are, up to now, the only stellar systems known to have deficient [Cu/Fe] ratios with respect to the trend in the Galactic disk and halo (McWilliam & Smecker-Hane 2005).

of the observational features of ω Centauri that appear so difficult to explain may find their natural place within a scenario like the one described above.

M.B. acknowledges the financial support of INAF through the Grant PRIN05 CRA 1.06.08.02. M.B. is grateful to the Observatoire de Strasbourg for the kind hospitality during the period in which most of the *N*-body simulations presented here have been performed. This work is partially based on observations made with the European Southern Observatory telescopes (WFI@2.2m) as part of the observing program 65.L-0463. Partially based on observations made with the ESO Very Large Telescope (VLT/FLAMES) as part of the observing program 075.D-0075. Partially based on Advanced Camera for Surveys (ACS) observations collected with the *HST* within the programme GO 10755. This research has made use of the NASA Astrophysics Data System Abstract Service.

Facilities: Keck (DEIMOS), ESO-VLT (FLAMES), MPG-ESO (WFI@2.2m), *HST* (ACS).

REFERENCES

Alard, C. 2001, A&A, 377, 389
Armandroff, T. E. 1989, AJ, 97, 375
Balcells, M., Graham, A. W., & Peletier, R. F. 2007, ApJ, 665, 1084
Bassino, L. P., & Muzzio, J. C. 1995, The Observatory, 115, 256
Bassino, L. P., Muzzio, J. C., & Rabolli, M. 1994, ApJ, 431, 634
Battaglia, G., Irwin, M., Tolstoy, E., Hill, V., Helmi, A., Letarte, B., & Jablonka, P. 2008, MNRAS, 383, 183
Bellazzini, M., Correnti, M., Ferraro, F. R., Monaco, L., & Montegriffo, P. 2006a, A&A, 446, L1
Bellazzini, M., Newberg, H. J., Correnti, M., Ferraro, F. R., Monaco, L., & Montegriffo, P. 2006b, A&A, 457, L21
Bellazzini, M., Ferraro, F. R., & Buonanno, R. 1999, MNRAS, 307, 619
Bellazzini, M., Ferraro, F. R., & Ibata, R. A. 2003a, AJ, 125, 188
Bellazzini, M., Ibata, R. A., Ferraro, F. R., & Testa, V. 2003b, A&A, 405, 577
Binggeli, B., Sandage, A., & Tammann, G. A. 1985, AJ, 90, 1681
Binggeli, B., Tammann, G. A., & Sandage, A. 1987, AJ, 94, 251
Böker, T. 2008, ApJ, 672, L111
Böker, T., Laine, S., van der Marel, R. P., Sarzi, M., Rix, H.-W., Ho, L., & Shields, J. C. 2004, AJ, 127, 105
Bonifacio, P., et al. 2006, in ESO Astrophysics Symposia, Chemical Abundances and Mixing in Stars in the Milky Wai and its Satellites, ed. S. Randich, & L. Pasquini (Berlin: Springer), 232
Boylan-Kolchin, M., & Ma, C.-P. 2004, MNRAS, 349, 1117
Brandt, S. 1970, Statistical and Computational Methods in Data Analysis (Amsterdam: North-Holland)
Brodie, J. P., & Strader, J. 2006, ARA&A, 44, 193
Brown, J. A., Wallerstein, G., & Gonzalez, G. 1999, AJ, 118, 1245
Burton, W. B., & Lockman, F. J. 1999, A&A, 349, 7
Carollo, C. M., Stiavelli, M., & Mack, J. 1998, AJ, 116, 68
Carraro, G., Zinn, R., & Moni Bidin, C. 2007, A&A, 466, 181
Carrera, R., Gallart, C., Pancino, E., & Zinn, R. 2007, AJ, 134, 1298
Carretta, E., & Gratton, R. 1997, A&AS, 121, 95
Catelan, M. 2008, Mem. SAH, 79, 388
Colpi, M., Mayer, L., & Governato, F. 1999, ApJ, 525, 720
Cordier, D., Pietrinferni, A., Cassisi, S., & Salaris, M. 2007, AJ, 133, 468
Côté, P., et al. 2006, ApJS, 165, 57 (C06)
Da Costa, G. S., & Armandroff, T. E. 1995, AJ, 109, 2533
Davis, M., et al. 2003, Proc. SPIE, 4834, 161
Dehnen, W. 2000, ApJ, 536, L39
Dehnen, W. 2002, J. Comput. Phys., 179, 27
Dehnen, W., & Binney, J. 1998, MNRAS, 294, 429
Dinescu, D. I, Girard, T. M., van Altena, W. F., & López, C. E. 2005, ApJ, 618, L25
Djorgovski, S. G., Gal, R. R., McCarthy, J. K., de Carvalho, R. R., Meylan, G., Bendinelli, O., & Parmeggiani, G. 1997, ApJ, 474, L19
Drinkwater, N. J., Gregg, M. D., Hilker, M., Bekki, K., Couch, W. J., Ferguson, H. C., Jones, J. B., & Phillipps, S. 2003, Nature, 423, 519
Evstigneeva, E. A., Gregg, M. D., Drinkwater, M. J., & Hilker, M. 2007, AJ, 133, 1722
Federici, L., Bellazzini, M., Galleti, S., Fusi Pecci, F., Buzzoni, A., & Parmeggiani, G. 2007, A&A, 473, 429
Ferguson, H. C., & Binggeli, B. 1994, A&A Rev., 6, 67
Ferrarese, L., & Côté, P. 2006, in IAU Symp. 238, Black Holes: from Stars to Galaxies—across the Range of Masses, ed. V. Karas, & G. Matt (Cambridge: Cambridge Univ. Press), 261 (FC06)
Freeman, K. C. 1993, in ASP Conf. Ser. 48, The Globular Cluster—Galaxy Connection, ed. G. H. Smith, & J. P. Brodie (San Francisco, CA: ASP), 608
Freeman, K. C., & Bland-Hawthorn, J. 2002, ARA&A, 40, 487
Fujii, M., Funato, Y., & Makino, J. 2006, PASJ, 58, 743
Gallagher, J. S., & Wyse, R. F. G. 1994, PASP, 106, 1225
Galleti, S., Federici, L., Bellazzini, M., Fusi Pecci, F., & Macrina, S. 2004, A&A, 416, 917
Geha, M., Guhathakurta, P., & van der Marel, R. P. 2002, AJ, 124, 3073
Geha, M., Guhathakurta, P., & van der Marel, R. P. 2003, AJ, 126, 1794
Gilmore, G., Wilkinson, M. I., Wyse, R. F. G., Kleyna, J. T., Koch, A., Wyn Evans, N., & Grebel, E. K. 2007, ApJ, 663, 948
Goerdt, T., Moore, B., Read, J. I., Stadel, J., & Zemp, M. 2006, MNRAS, 368, 1073
Graham, A. W., & Guzmán, R. 2003, AJ, 125, 2936
Grant, N. I., Kuipers, J. A., & Phillipps, S. 2005, MNRAS, 363, 1019
Harbeck, D., et al. 2001, AJ 3092
Hargreaves, J. C., Gilmore, G., & Annan, J. D. 1996, MNRAS, 279, 108
Harris, W. E 1996, AJ, 112, 1487
Hasegan, M., et al. 2005, ApJ, 627, 203
Hernandez, X., & Gilmore, G. 1998, MNRAS, 297, 517
Ibata, R., Chapman, S., Ferguson, A., Lewis, G., Irwin, M., & Tanvir, N. 2005, ApJ, 634, 287
Ibata, R., & Lewis, G. 1998, ApJ, 500, 575
Ibata, R., Lewis, G., Irwin, M., Totten, E., & Quinn, T. 2001, ApJ, 551, 294
Ibata, R. A., Irwin, M. J., & Gilmore, G. 1994, Nature, 370, 194
Ibata, R. A., Wyse, R. F. G., Gilmore, G., Irwin, M. J., & Suntzeff, N. B. 1997, AJ, 113, 634
Illingworth, G. 1976, ApJ, 204, 73
Illingworth, G., & Illingworth, W. 1976, ApJS, 30, 227
King, I. R. 1962, AJ, 67, 471
King, I. R. 1966, AJ, 71, 64
Layden, A. C., & Sarajedini, A. 2000, AJ, 119, 1760 (LS00)
Lotz, J. M., Miller, B. W., & Ferguson, H. C. 2004, ApJ, 613, 262
Lotz, J. M., Telford, R., Ferguson, H. C., Miller, B. W., Stiavelli, M., & Mack, J. 2001, ApJ, 572
Lupton, R. 1993, in Statistics in Theory and Practice (Princeton, NJ: Princeton Univ. Press)
Mackey, A. D., & Gilmore, G. F. 2003, MNRAS, 340, 175
Mackey, A. D., & van den Bergh, S. 2005, MNRAS, 360, 631
Majewski, S. R., Skrutskie, M. F., Weinberg, M. D., & Ostheimer, J. C. 2003, ApJ, 599, 1082
Mandushev, G., Staneva, A., & Spasova, N. 1991, A&A, 252, 94
Martin, N. F., Ibata, R. A., Chapman, S. C., Irwin, M. J., & Lewis, G. F. 2007, MNRAS, 380, 281
Maschenko, S., & Sills, A. 2005, ApJ, 619, 243
Mayer, L., Kzantzidis, S., Mastropiero, C., & Waldsley, J. 2007, Nature, 445, 738
McLaughlin, D. E., & van der Marel, R. P. 2005, ApJS, 161, 304
McWilliam, A., & Smecker-Hane, T. 2005, ApJ, 622, L29
Mieske, S., & Baumgardt, H. 2007, A&A, 475, 851
Milgrom, M. 2008, in Matter and energy in the Universe: from nucleosynthesis to cosmology, XIX Rencontres de Blois, in press (arXiv:0801.3133)
Miocchi, P., Capuzzo Dolcetta, R., Di Matteo, P., & Vicari, A. 2006, ApJ, 644, 940
Monaco, L., Bellazzini, M., Bonifacio, P., Buzzoni, A., Ferraro, F. R., Marconi, G., Sbordone, L., & Zaggia, S. 2007, A&A, 464, 201
Monaco, L., Bellazzini, M., Ferraro, F. R., & Pancino, E. 2003, ApJ, 597, L25
Monaco, L., Bellazzini, M., Ferraro, F. R., & Pancino, E. 2003, ApJ, 597, L25
Monaco, L., Bellazzini, M., Ferraro, F. R., & Pancino, E. 2005a, MNRAS, 356, 1396 (M05a)
Monaco, L., Bellazzini, M., Bonifacio, P., Ferraro, F. R., Marconi, G., Pancino, E., Sbordone, L., & Zaggia, S. 2005b, A&A, 441, 141 (M05b)
Monaco, L., Ferraro, F. R., Bellazzini, M., & Pancino, E. 2002, ApJ, 578, L47
Montegriffo, P., Bellazzini, M., Ferraro, F. R., Martins, D., Sarajedini, A., & Fusi Pecci, F. 1998, MNRAS, 294, 315
Muñoz, R. R., Majewski, S. R., & Johnston, K. V. 2008, ApJ, 679, 346
Navarro, J. F., Frenk, C. S., & White, S. D. M. 1996, ApJ, 462, 563 (NFW)
Norris, J. E., Freeman, K. C., Mayor, M., & Seitzer, P. 1997, ApJ, 487, L187
Noyola, E., & Gebhardt, K. 2006, AJ, 132, 447
Oh, K. S., Lin, D. N. C., & Richer, H. B. 2000, ApJ, 531, 727
Olszewski, E. W., Pryor, C., & Armandroff, T. E. 1996, AJ, 111, 750

Pancino, E., Ferraro, F. R., Bellazzini, M., Piotto, G., & Zoccali, M. 2000, ApJ, 534, L83
Pancino, E., Pasquini, L., Hill, V., Ferraro, F. R., & Bellazzini, M. 2002, ApJ, 568, L101
Pancino, E., Seleznev, A., Ferraro, F. R., Bellazzini, M., & Piotto, G. 2003, MNRAS, 345, 683
Peterson, C. J. 1993, in ASP Conf. Ser. 50, Structure and Dynamics of Globular Clusters, ed. S. Djorgovsky, & G. Meylan (San Francisco, CA: ASP), 337
Pryor, C., & Meylan, G. 1993, in ASP Conf. Ser. 50, Structure and Dynamics of Globular Clusters, ed. S. Djorgovsky, & G. Meylan (San Francisco, CA: ASP), 357
Read, J. I., Goerdt, T., Moore, B., Pontzen, A. P., Stadel, J., & Lake, G. 2006, MNRAS, 373, 1451
Renzini, A., & Buzzoni, A. 1986, in Spectral Evolution of Galaxies, (Dordrecht: Reidel), 195
Renzini, A., & Fusi Pecci, F. 1988, ARA&A, 26, 199
Rix, H.-W., de Zeeuw, P. T., Cretton, N., van der Marel, R. P., & Carollo, M. 1997, AJ, 488, 702
Robin, A. C., Reylé, C., Derrière, S., & Picaud, S. 2003, A&A, 409, 523
Rossa, J., van der Marel, R. P., Böker, T., Gerssen, J., Ho, L. C., Rix, H.-W., Shields, J. C., & Walcher, C.-J. 2006, ApJ, 132, 1074
Sánchez-Salchedo, F. J., Reyes Iturbide, J., & Hernandez, X. 2006, MNRAS, 370, 1829
Sanders, R. H., & McGaugh, S. S. 2002, ARA&A, 40, 263
Sarajedini, A., & Layden, A. C. 1995, AJ, 109, 1086
Sarajedini, A., & Layden, A. C. 1997, AJ, 113, 264
Sarajedini, A., et al. 2007, AJ, 133, 1658
Siegel, M. H., et al. 2007, ApJ, 667, L57
Sollima, A., Beccari, G., Ferraro, F. R., Fusi Pecci, F., & Sarajedini, A. 2007, MNRAS, 380, 781
Strigari, L. E., Bullock, J. S., Kaplinghat, M., Kravtsov, A. V., Gnedin, O. Y., Abazajian, K., & Klypin, A. A. 2006, ApJ, 652, 306
Teuben, P. J. 1995, in ASP Conf. Ser. 77, Astronomical Data Analysis Software and Systems IV, ed. R. Shaw, H. E. Payne, & J. J. Hayes (San Francisco, CA: ASP), 398
Trager, S. C., King, I. R., & Djorgovski, S. G. 1995, AJ, 109, 218
van Leeuwen, F., Hughes, J. D., & Piotto, G. 2002, in ASP Conf. Ser. 265, ω Centauri, A Unique Window into Astrophysics (San Francisco, CA: ASP)
Valluri, M., Ferrarese, L., Meritt, D., & Joseph, C. L. 2005, ApJ, 628, 137
van de Ven, G., van den Bosch, R. C. E., Verolme, E. K., & de Zeeuw, P. T. 2006, A&A, 445, 513
Walker, M. G., Mateo, M., Olszewki, E. W., Bernstein, R., Wang, X., & Woodroofe, M. 2006, AJ, 131, 2114
Webbink, R. F. 1985, in IAU Symp. 113, Dynamics of Star Clusters, ed. J. Goodman, & P. Hut (Dordrecht: Kluwer), 541
Wehner, E. H., & Harris, W. E. 2006, ApJ, 644, L17